



#### Available online at www.sciencedirect.com

### **ScienceDirect**

Geochimica et Cosmochimica Acta 310 (2021) 1-18

### Geochimica et Cosmochimica Acta

www.elsevier.com/locate/gca

## Vertical patterns of phosphorus concentration and speciation in three forest soil profiles of contrasting climate

Zhuojun Zhang <sup>a,b,h</sup>, Zhiqi Zhao <sup>c</sup>, Congqiang Liu <sup>d</sup>, Oliver A. Chadwick <sup>e</sup>, Chao Liang <sup>f</sup>, Yongfeng Hu <sup>g</sup>, Karen L. Vaughan <sup>b</sup>, Mengqiang Zhu <sup>b,\*</sup>

<sup>a</sup> State Key Laboratory of Environmental Geochemistry, Institute of Geochemistry, Chinese Academy of Sciences, Guiyang, Guizhou 550081, China

b Department of Ecosystem Science and Management, University of Wyoming, Laramie, Wyoming 82071, United States

<sup>c</sup> School of Earth Science and Resources, Chang'an University, Xi'an, Shaanxi 710054, China

<sup>d</sup> Institute of Surface-Earth System Sciences, Tianjin University, Tianjin 300072, China

<sup>e</sup> Geography Department, University of California, Santa Barbara, California 93106, United States

<sup>f</sup> Institute of Applied Ecology, Chinese Academy of Sciences, Shenyang, Liaoning 110016, China

<sup>g</sup> Canadian Light Source Inc., University of Saskatchewan, Saskatoon, Saskatchewan S7N 2V3, Canada

<sup>h</sup> University of Chinese Academy of Sciences, Beijing 100049, China

Received 10 February 2021; accepted in revised form 1 July 2021; available online 08 July 2021

#### Abstract

Phosphorus (P) availability in soils controls critical functions and properties of terrestrial ecosystems. Vertical distribution patterns of P concentration and speciation in soil profiles provide historical records of how pedogenic processes redistribute and transform P and thus change its availability in soils, which, however, remain poorly understood. We determined the patterns in three forest soil profiles of contrasting climate, using fine sampling intervals, P K-edge X-ray absorption near edge (XANES) spectroscopy and chemical extractions. The major features of the patterns persist under the contrasting climate. The total P concentration decreases from A to B horizons, reaches a minimum in the B horizons, and then increases towards the upper C horizons, but with little variations with depth in the lower C horizons. Both calcium-bound inorganic P (Ca-P<sub>1</sub>) and organic  $P(P_0)$  decrease and Fe- and Al-bound  $P_i$  [(Fe + Al)- $P_i$ ] increases in proportion downward in the A horizons because dust inputs and accumulation of organic matter both decline with increasing depth. Ca-Pi is negligible and (Fe + Al)-P<sub>i</sub> is dominant in the B horizons due to strong weathering. There is a strong downward increase in Ca-P<sub>i</sub> proportion and decrease in  $(Fe + Al)-P_i$  proportion from the lower B to the upper C horizons. New Ca-P<sub>i</sub> seems to form in the upper C horizons where downward leaching Ca<sup>2+</sup> and phosphate accumulate due to the low water permeability of the soils. In the lower C horizons, Ca-P<sub>i</sub> increases and (Fe + Al)-P<sub>i</sub> decreases with increasing depth due to decreasing chemical weathering. Regarding P bioavailability, the proportion of occluded P (Pocc) shows an increasing and decreasing trend with increasing depth, being the highest in the B horizons; however, there are no consistent trends for non-occluded P ( $P_{n-occ}$ ). While the P vertical patterns can be understood by considering the relative importance of different pedogenic processes, climate affects the intensities of these processes and thus the details of the patterns. When depth-integrated, warmer/wetter climate results in decreases in the proportions of both  $Ca-P_i$  and  $P_{n\text{-}occ}$  but increases in the P loss and the proportions of  $P_o$ ,  $(Fe+Al)-P_i$ , and  $P_{occ}$ . Regardless of soil depth and climate, the  $P_i$  speciation, i.e., the relative proportions of  $Ca-P_i$  and  $(Fe+Al)-P_i$  over total P<sub>i</sub>, correlates well with soil pH and weathering degree (Chemical Index of Alteration, CIA), and the P<sub>o</sub> concentration correlates with pedogenic Fe and Al and organic carbon concentration. The correlations suggest that the P<sub>i</sub> speciation is primarily controlled by soil geochemistry/mineralogy, and the Po concentration by both soil geochemistry/mineralogy and biological activities. Pocc correlates with CIA, and thus is mainly controlled by soil mineralogy; but Pn-occ correlates weakly with soil

E-mail address: mzhu6@uwyo.edu (M. Zhu).

<sup>\*</sup> Corresponding author.

properties, probably due to its susceptibility to combined influences of dust inputs, leaching, biological activities, and adsorption on minerals. The above quantitative relationships may help predict P speciation and availability in diverse soils. We further show that soil profiles, and climate and CIA gradients are useful tools for studying P transformations, particularly for the  $P_i$  pool, during pedogenesis. This study provides an integration and synthesis of controls of climatic and edaphic variables on P dynamics in forest soils.

© 2021 Elsevier Ltd. All rights reserved.

Keywords: Phosphorus speciation; Concentration and availability; Soil profiles; Vertical patterns; Climate; XANES spectroscopy

#### 1. INTRODUCTION

Phosphorus (P) is an essential nutrient element (Elser et al., 2007; Filippelli, 2008), and its bioavailability represents a key control on primary productivity, plant diversity and microbial decomposition (Föllmi, 1996; Tyrrell, 1999; Elser et al., 2007; Filippelli, 2008). Phosphorus in terrestrial ecosystems is ultimately derived from rock weathering. Once P is released into soil by rock weathering, it is distributed among multiple chemical species that differ in mobility and bioavailability. Steep physical, chemical and biological gradients in soil profiles can strongly affect the vertical spatial distribution patterns of P concentration and speciation, which in turn govern P availability and constrain biological activity at different depths of soils. Thus, the vertical distribution patterns can yield insights into what biogeochemical and physical processes control P chemistry, mobility and bioavailability in each soil layer, as well as its mass exchange within the profile, and between the profile and its surrounding environment. However, the vertical distribution patterns and the controlling physical and biogeochemical processes, particularly under contrasting climate, are not fully understood.

Phosphorus vertical distribution patterns in nonagricultural soil profiles are affected by physical and chemical weathering, material transport (eluviation and illuviation), biological activities, and external inputs, such as aeolian dust inputs (Jobbágy and Jackson, 2001; Pett-Ridge, 2009; Porder and Chadwick, 2009; Brantley and Lebedeva, 2011; Aciego et al., 2017; Arvin et al., 2017; Hasenmueller et al., 2017; Zhou et al., 2018; Gu et al., 2019). For undisturbed natural ecosystems, some weathering profiles displayed a considerable loss of P from soil A and B horizons relative to the bedrock due to weathering, plant uptake, erosion, leaching and runoff (St. Arnaud et al., 1988; Jobbágy and Jackson, 2001; Eger et al., 2011; Mishra et al., 2013), while others showed a slight loss or even a gain of P in the A horizons ascribed to organic P accumulations and/or aeolian dust inputs (St. Arnaud et al., 1988; Jobbágy and Jackson, 2001; Prietzel et al., 2016; Aciego et al., 2017).

The vertical stratification of soil properties across a soil profile results in distinct P speciation at each layer (Walker and Syers, 1976; St. Arnaud et al., 1988; Jobbágy and Jackson, 2001; Ippolito et al., 2010; Eger et al., 2011; Mishra et al., 2013). Using P K-edge X-ray absorption near edge structure (XANES) spectroscopy, Prietzel et al. (2016) found that Fe- and Al-bound P [(Fe + Al)-P, including both organic (P<sub>o</sub>) and inorganic (P<sub>i</sub>) phosphates adsorbed

to Fe and Al minerals, i.e.,  $(Fe + Al)-P_i + (Fe + Al)-P_o$ was dominant in A and B horizons of forest soil profiles formed from silicate bedrock or loess, whereas Ca-bound inorganic P (Ca-P<sub>i</sub>) dominated in the C horizons. The P speciation of calcareous forest soils was dominated by Ca-bound organic P (Ca-P<sub>o</sub>) and free P<sub>o</sub> (not bound to metals) (Prietzel et al., 2016). Werner et al. (2017) investigated the influence of podzolization intensity in temperate forest soils formed from silicate bedrock on the spatial distribution of P species in soil profiles using chemical extractions. They found that P bound to primary silicate minerals decreased due to desorption of phosphate and displacement by other soil solution anions with increasing podzolization (Werner et al., 2017). Chemical extractions showed that for grassland soil profiles, P accumulated as Po in surface soils primarily due to accumulation of grass roots, while total P was depleted and Ca-P; decreased in the subsurface (St. Arnaud et al., 1988; Ippolito et al., 2010). In addition, aeolian dust deposition is a global phenomenon (Mahowald et al., 2008), which can increase total P and Ca-P<sub>i</sub> in soil profiles (Crews et al., 1995; Eger et al., 2013; Gu et al., 2019). The degrees of the increase depend on the chemical composition of dust and the relative magnitude of dust input and soil weathering intensity (Gu et al., 2019). In agricultural soils, P speciation as determined from P K-edge XANES analyses was dominated by both Po and (Fe + Al)-P<sub>i</sub> in the topsoil, with a higher proportion of (Fe + Al)- $P_i$  in the subsoil; ~90% of the total P was apatite-derived in deeper soils (Amelung et al., 2015; Eriksson et al., 2016; Koch et al., 2018; Glæsner et al., 2019; Baumann et al., 2020). Based on chemical extractions, Mishra et al. (2013) and Newman et al. (2020) further concluded that the P vertical patterns in a soil profile were analogous to the P transformation patterns as a function of soil developmental time (using soil chronosequences) as described in the Walker and Syers model (Walker and Syers, 1976). In this mode, the total P concentration decreased and the proportion of Ca-P<sub>i</sub> declined, with concurrent increases in Po and (Fe + Al)-Pi proportions towards the more weathered soils during soil development (Walker and Syers, 1976).

However, most of the previous studies on the vertical distribution patterns of P speciation used chemical extractions to characterize P pools in soil profiles (St. Arnaud et al., 1988; Miller et al., 2001; Ippolito et al., 2010; Eger et al., 2011; Emadi et al., 2012; Mishra et al., 2013; Amelung et al., 2015; Werner et al., 2017). The chemical extractions operationally define P pools and do not provide accurate information on P speciation (Negassa and

Leinweber, 2009; Kar et al., 2011; Gu et al., 2020). Thus, the use of extractions may lead to large uncertainties in defining P geochemistry in soil profiles. Phosphorus Kedge XANES spectroscopy is believed to be a more accurate method in charactezing soil P speciation (Hesterberg et al., 1999; Beauchemin et al., 2003; Sato et al., 2005; Ingall et al., 2011; Prietzel et al., 2013; Kraal et al., 2015). To date, only one study reported P K-edge XANES analysis of P speciation in forest soil profiles (Prietzel et al., 2016), which focused on P speciation methodologically and the relationship of P species with parent material, and solely studied soil horizons. Moreover, the soil profiles studied in previous studies were down to 1-m depth, and P distribution and transformations in the deeper layers were unknown (Buss et al., 2010; Newman et al., 2020). In addition, previous studies used coarse sampling depth intervals (i.e., 20 cm, Jobbágy and Jackson, 2001), or collected a single soil sample per soil horizon (e.g., Amelung et al., 2015; Eger et al., 2011; Prietzel et al., 2016; St. Arnaud et al., 1988), potentially missing important P distribution features.

Climate is one of the five soil forming factors (Jenny, 1941), and can strongly affect weathering intensity, soil chemistry and mineralogy, leaching, and biological activities. Warmer/wetter climatic conditions result in more weathered soils with lower pH, increased formation of secondary minerals, and increased loss of many bedrockderived elements. These changes in soil chemical and mineralogical properties affect soil P stock, chemistry and availability (Miller et al., 2001; Ippolito et al., 2010; Emadi et al., 2012; Feng et al., 2016; Deiss et al., 2018; Hou et al., 2018). With increasing mean annual precipitation (MAP, 34-884 mm for grasslands, or 550-1250 mm for forests), Ca-P<sub>i</sub> was found to decrease while both P<sub>o</sub> and occluded P (Pocc) increased in proportion in topsoil (Ippolito et al., 2010; Emadi et al., 2012; Feng et al., 2016). In volcanic forest topsoil, (Fe + Al)-P<sub>i</sub> declined and Po increased with increasing MAP from 1500 mm to 5000 mm because of dissolution loss of Fe and Al minerals at high rainfall levels (Miller et al., 2001). Based on a global database and a meta-analysis across a wide range of terrestrial ecosystems, Hou et al. (2018) indicated that MAP had a relatively minor effect on available P, while mean annual temperature (MAT, -5 to 29 °C) negatively affected available P mainly by decreasing Po and Ca-Pi and increasing soil sand content. No systematic studies have been reported regarding climatic effects on vertical distribution patterns of P concentration and speciation in soil profiles.

Given that soil properties ultimately control P speciation and availability, Hou et al. (2018) also reported the relationships between edaphic variables and P pools using the global database. They found that soil pH positively correlated with primary mineral P and negatively with secondary mineral P. All soil P pools (i.e., primary mineral P, secondary mineral P, available P and P<sub>o</sub>) negatively correlated with soil sand content but positively correlated with soil organic carbon (SOC). However, the above relationships were obtained based on chemical extractions and the relationships between P speciation and edaphic variables have not been determined.

Forest ecosystems, which cover about 31% of Earth's land surface and play a major role in global biogeochemical cycles (FAO, 2015), are often limited by P (Vitousek and Sanford, 1986; Vitousek et al., 2010). In the present study, we determined P vertical concentration, speciation and availability patterns in soil profiles of three forest ecosystems of contrasting climate using fine sampling depth intervals and a combination of P K-edge XANES spectroscopic and chemical extraction analyses. A variety of soil chemical and mineralogical properties were measured, which assist in the interpretations of the P patterns. A one-dimensional conceptual model was further proposed for the vertical P concentration and speciation patterns. We also identified the edaphic variables that strongly affect P speciation and availability regardless of soil depth and climatic conditions. The relationships were quantified and can be useful for predicting soil P speciation and availability for other soils. Our dataset further allowed us to discuss the use of soil profiles and climate gradients for studying P biogeochemical transformations during soil development. Overall, the present study provides an integration and synthesis of controls of climatic and edaphic variables on P concentration, speciation and availability in forest soils.

#### 2. MATERIALS AND METHODS

#### 2.1. Study sites and soil sampling

Three soil profiles developed on granite were respectively located in Orogen Autonomous Banner, Inner Mongolia; Oinhuangdao, Hebei; and Ledong, Hainan in China (Fig. 1a). These sites spread from northeast to southeast China, spanning 30° of latitude, and thus named as NE (northeast), MID (middle), and SE (southeast), respectively. The MAT ranged from -0.4 °C to 25 °C and MAP from 480 mm to 1500 mm (Table A1). The NE profile was located in a sub-humid mid-temperate climate with a MAT of -0.4 °C and MAP of 480 mm. The site was covered with broadleaf forest. The MID profile was in a humid warm-temperate climate with a MAT of 11 °C and MAP of 640 mm. The vegetation type of the site was deciduous broadleaf forest. The SE profile was located in a tropical hot and humid climate with a MAT of 25 °C and MAP of 1500 mm. The rainy season at this site extends from December to May and the driest period normally occurs between August and October. The site was dominated by evergreen broadleaf trees.

The three profiles, exposed as fresh road cuts, were sampled from top to bottom with fine depth intervals (5 or 10 cm). The soil profiles were minimally impacted by human activities because they were fresh and located in remote regions. They were also distant from agricultural areas so that contamination from P fertilization is unlikely. Little disturbance from human earthworks and agricultural activities is further implied by the contiguous changes in pH, SOC, and pedogenic Fe and Al concentrations with depth in all three profiles (data given below).

The slopes of the NE, MID and SE profiles were 10°, 2°, and 3° and the sampled profile thicknesses were 3, 3.6 and 7 m, respectively. Soil horizons were designated according

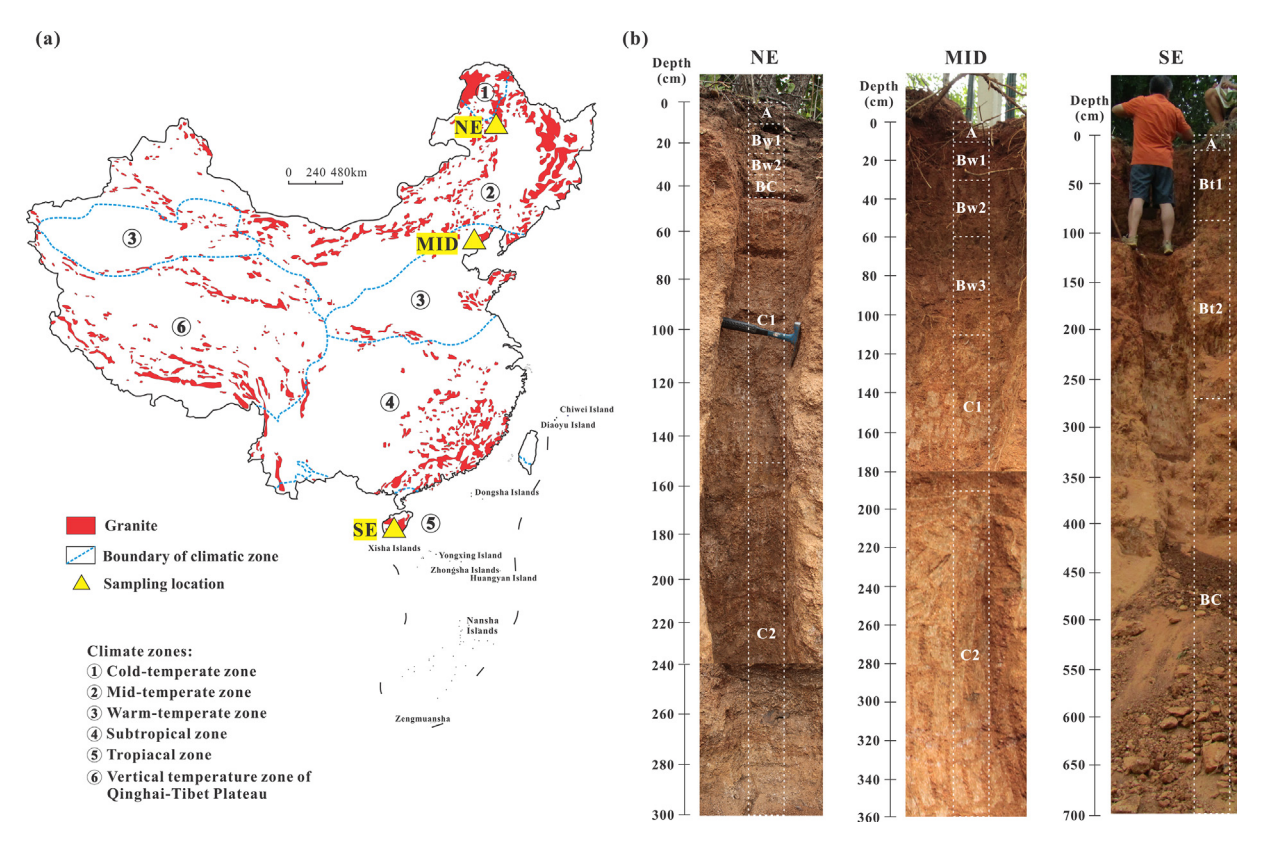


Fig. 1. (a) The locations of the sampling sites with soils formed in granitic bedrock in China, including Oroqen Autonomous Banner, Inner Mongolia (NE); Qinhuangdao, Hebei (MID); and Ledong, Hainan (SE). (b) The photos of the soil profiles with horizon designation and depth (Also see Table A2).

to the United States Soil Taxonomy (Soil Survey Staff, 2014), including A, B and C horizons for the NE and MID profiles but only A and B horizons for the SE profile because the C horizons were too deep to sample (Fig. 1b, Table A2). The soils of both NE and MID were classified as Ustic Dystrocryepts, and SE soil as a Typic Hapludox (Soil Survey Staff, 2014). Granite bedrock samples were collected from the outcrops nearby each soil profile. Major minerals in the granite samples were quartz, plagioclase, K-feldspar and biotite, and minor minerals included hornblende and chlorite (Cui, 2014).

The three profiles differed in soil residence time (SRT) which was defined as the average time that a particle resides in a soil profile after formation from bedrock but before erosion (Dere, 2014). SRT is a good estimate for the duration of time that soil particles remain in the weathering zone. SRT can be calculated from the profile thickness (h) and the denudation rate (D):

$$SRT = \frac{h}{D} \tag{1}$$

The denudation rates of NE, MID and SE profiles were 31, 14, and 59 m/Myr (or 55.3, 29.2 and 94.7 g m<sup>-2</sup> yr<sup>-1</sup>), respectively, based on cosmogenic <sup>26</sup>Al and <sup>10</sup>Be concentrations measured in quartz from the three soil profiles (Cui et al., 2014; Cui, 2014). The SRTs of NE, MID and SE profiles were estimated to be 97, 257, and 119 kyr, respectively. Climate fluctuated during the glacial-interglacial cycles over those time periods (Huang et al., 2018).

All three profiles received aeolian dust inputs. Strontium isotope data indicated that the upper part of the NE profile received substantial amounts of dust inputs (1.2–19.3% soil mass contributions) (Fig. A1). Although we did not determine the dust contribution to the MID and SE profiles, Li et al. (2016) found that the soil profiles geographically near the SE profile had high dust mass contributions (12–58%) as well.

#### 2.2. Characterization of soil properties

The bulk densities of the soils were determined on moist soils using the core method (EA-1, Blake and Hartge, 1986). The remaining field moist soils were air-dried and passed through 2-mm mesh sieves. The <2 mm samples were analyzed for pH with 1:2.5 soil/CO<sub>2</sub>-free deionized water. Subsamples of the sieved soils and the granite rock samples were ball-milled to <200 mesh (75  $\mu$ m) for measuring concentrations of major elements, pedogenic Fe and Al minerals, and SOC as well as for modified Hedley sequential extractions and P K-edge XANES spectroscopy.

Major elements were determined by inductively coupled plasma-optical emission spectroscopy (ICP-OES, Perkin Elmer Optima 8300) after lithium tetraborate fusion at 1,000 °C for 60 min followed by 5% aqua regia digestion of the fusion beads (Robertson et al., 1999). Both the precision and accuracy were about 5%. The SOC concentrations were determined with an elemental analyzer (vario MACRO cube, ELEMENTAR) after decarbonation.

Pedogenic Fe and Al were quantified by two-step extractions using acidic (pH 3.2) ammonium oxalate solution (Fe<sub>ox</sub>, Al<sub>ox</sub>) (Schwertmann, 1964), followed by citrate-dithionite solution (Fe<sub>di</sub>, Al<sub>di</sub>) (Holmgren, 1967). The detailed procedures are provided in EA-1. The total contents of pedogenic Fe (Fe<sub>ox+di</sub>) and Al (Al<sub>ox+di</sub>) and associated P were calculated as the sum of oxalate and dithionate extractable Fe, Al and P, respectively.

The degree of P saturation (DPS $_{ox}$ ) of each soil, defined as the ratio of the amount of adsorbed P to the P sorption capacity of the soil, was used to evaluate the potential of soils to release P (Hooda et al., 2000). DPS $_{ox}$  was calculated on a molar basis using the following formula:

$$DPS_{ox} = \frac{P_{ox}}{Al_{ox} + Fe_{ox}} \times 100 \tag{2}$$

Degree of chemical weathering was indicated by the Chemical Index of Alteration (CIA) (Nesbitt and Young, 1982):

$$CIA = \frac{Al_2O_3}{Al_2O_3 + CaO^* + Na_2O + K_2O} \times 100$$
 (3)

where all constituent concentrations are expressed in moles/kg. CaO\* refers to the CaO only incorporated in silicates, not in apatite and carbonate, and is corrected using the method of McLennan (1993).

The titanium (Ti)-normalized P concentration  $(\tau_P)$  was used to estimate the P losses and gains in the profile relative to bedrock (Brimhall and Dietrich, 1987; Anderson et al., 2002):

$$\tau_P = \frac{[P]_w \times [Ti]_p}{[P]_p \times [Ti]_w} - 1 \tag{4}$$

where [P] and [Ti] are the concentrations of total P and the relatively immobile element Ti respectively, and the subscripts w and p refer to the weathered soils and bedrock, respectively.  $\tau_P$  indicates P loss ( $\tau_P < 0$ ) or gain ( $\tau_P > 0$ ) relative to the composition of the bedrock. To use the equation to calculate mass balance, aeolian inputs must have a negligible effect on Ti concentrations in soils, which is the case when aeolian fluxes are smaller than total denudation rates and Ti concentrations in aeolian dust are comparable to those in the chemically weathered rock (Riebe et al., 2001; Riebe et al., 2003). For the NE profile that was close to the Chinese loess plateau, the denudation rate was  $55.3~{\rm g~m^{-2}~yr^{-1}}$ , much higher than the dust deposition rate  $0.46~{\rm g~m^{-2}~yr^{-1}}$  estimated from the Sr isotopic composition (EA-2). Other two sites presumably had lower dust inputs than the NE site because they were further away from dust source regions (i.e., 0.06–0.13 g m<sup>-2</sup> yr<sup>-1</sup> for the SE site) (Li et al., 2016), and thus, the aeolian fluxes were expected to be much smaller than the denudation rates as well. Meanwhile, the soil Ti concentrations of the three profiles (~3202, ~3524, and ~4841 µg/g for the NE, MID and SE profiles, respectively) were similar to those in the dust (3028–5488 µ g/g) (Xie and Chi, 2016). Thus, the gain and loss of P in the three profiles under small dust inputs can be approximately estimated using the mass balance approach (Bullen and Chadwick, 2015; Buss et al., 2017; Li et al., 2020; Rea et al., 2020), although additional parameters need to be

considered to incorporate dust inputs into the mass balance model (Ferrier et al., 2011).

The percentage of depth-integrated P gain or loss in the entire profile was calculated to evaluate P gain or loss from the entire profile relative to bedrock (Chadwick et al., 1990):

P gain or loss (%) = 
$$\frac{\sum_{k=1}^{n} \tau_{P(k)} \Delta h_{(k)}}{h} \times 100$$
 (5)

where *n* refers to the number of soil layers,  $\Delta h$  refers to the layer thickness, and *h* refers to the profile thickness,  $h = \sum_{k=1}^{n} \Delta h_{(k)}$ .

### 2.3. Phosphorus K-edge XANES spectroscopy

Phosphorus K-edge XANES spectra were collected from the soil samples at the Soft X-ray Micro-Characterization Beamline (SXRMB) at the Canadian Light Source, Saskatoon, Canada. The characteristics of the equipment and the scanning parameters were the same as used in our previous study (Gu et al., 2019). The beamline was equipped with a Si(1 1 1) double-crystal monochromator. The beamline energy was calibrated using Ar K-edge at 3205 eV, and the main peak position of AlPO<sub>4</sub> was set at 2152.9 eV. Phosphate references, either purchased or synthesized according to the previous studies (Zhang et al., 2018; Gu et al., 2019), were used for the linear combination fitting (LCF) analysis, including poorly-crystalline apatite (Ca-P<sub>i</sub>), ferrihydrite-adsorbed PO<sub>4</sub> (Fe-P<sub>i</sub>), amorphous FePO<sub>4</sub> (Fe-P<sub>i</sub>), kaolinite-adsorbed PO<sub>4</sub> (Al-P<sub>i</sub>), berlinite (AlPO<sub>4</sub>, Al-P<sub>i</sub>), and phytic acid sodium salt (organic P, P<sub>o</sub>) (Fig. A2). The phosphate reference compounds with high P concentration were measured in electron yield mode to avoid self-absorption that otherwise would occur if data were collected in fluorescence mode using a four-element Si-drift fluorescence detector. The energy range of each scan was set from 2119.5 to 2210 eV with a 2 eV step size from 2119.5 to 2143 eV, 0.15 eV from 2143 to 2175 eV, and 0.75 eV from 2175 to 2210 eV. The dwelling time at each step varied from 1.0 to 16 s. All samples were scanned at least twice, and the spectra were averaged to improve signal-to-noise ratios. The average spectra were background removed, normalized and then subject to the LCF analysis to quantify the relative proportions of various P species using ATHENA (Ravel and Newville, 2005). All spectra were background corrected by a linear regression fit through the pre-edge region (2125-2140 eV) and a polynomial regression fit through the post-edge region (2174-2210 eV) for normalization. The LCF analysis was performed over 2140-2190 eV and energy shift was not allowed during the fitting. The sum of the fractions of the P references used was not forced to one during the fitting, but the sum of the obtained fractions was normalized to one. The goodness-of-fit was evaluated by R-factor, and P references yielding the best fit were considered as the most possible P species in the samples. Four or fewer P reference compounds were chosen to prevent overfitting.

Ca-P<sub>i</sub> can be well quantified by the XANES-LCF analysis due to its distinct spectral features, including a lower white-line energy, a stronger shoulder on the right side of

white-line peak and stronger splitting of post-edge peak compared to other references (Fig. A2) (Barrow et al., 2020; Gu et al., 2020). The XANES spectroscopy, however, may be unable to accurately quantify (Fe+Al)-P<sub>i</sub> due to its similar spectra to that of (Fe+Al)-Po (Prietzel and Klysubun, 2018). Consequently, when using Ca-P<sub>i</sub>, (Fe+Al) P<sub>i</sub> and free P<sub>o</sub> compounds as the only references for a XANES-LCF analysis, like in this study, (Fe+Al)-P<sub>i</sub> would be overestimated by including some (Fe+Al)-Po; meanwhile, total Po is underestimated due to its loss of (Fe+Al)-P<sub>o</sub> to the (Fe+Al)-P<sub>i</sub> pool. Given the uncertainty of the XANES-LCF analysis for Po, chemical extractions are likely the more accurate method for quantifying total  $P_o$  [including both free  $P_o$  and  $(Fe + Al)-P_o$ ] in soils (Prietzel et al., 2016). In the present study, the total P<sub>o</sub> concentration was obtained from chemical extractions. We defined the difference between the extraction- and XANES-determined Po proportions as the proportion of the P<sub>o</sub> bound to Fe and Al, i.e., (Fe + Al)-P<sub>o</sub> as below.

$$f_{\text{(Fe+Al)-Po}} = f_{\text{Po-extraction}} - f_{\text{Po-XANES}} \tag{6}$$

where  $f_{\text{Po-extraction}}$  is the percentage of total  $P_{\text{o}}$  over total  $P_{\text{o}}$  determined from chemical extractions and  $f_{\text{Po-XANES}}$  is determined from the XANES-LCF analysis. The proportion of  $(\text{Fe} + \text{Al}) - P_{\text{i}}$  was calculated as below.

$$f_{\text{(Fe+Al)-Pi}} = 100 - f_{\text{Ca-Pi}} - f_{\text{Po-extraction}} \tag{7}$$

where  $f_{\text{Ca-Pi}}$  is the percentage of Ca-P<sub>i</sub> obtained from the XANES-LCF analysis and  $f_{\text{Po-extraction}}$  is the percentage of total P<sub>o</sub>, over total P, determined from chemical extractions. The above strategy to obtain P speciation assumed that Ca-bound P<sub>o</sub> was negligible as demonstrated in Prietzel et al. (2016).

The depth-integrated mass proportion of each P species *i* was calculated by integrating the soil depth to evaluate the contribution of various P species to the total P stock in the soil horizons:

Mass proportion of P species i

$$= \frac{\sum_{k=1}^{n} C_{P \ species \ i(k)} \rho_{(k)} \Delta h_{(k)}}{\sum_{k=1}^{n} C_{P(k)} \rho_{(k)} \Delta h_{(k)}}$$
(8)

where n refers to the number of soil layers,  $\Delta h$  refers to the layer thickness, and  $\rho$  refers to the bulk density.  $C_{P \, species \, i(k)}$  is the concentration of P specie i of the  $k^{th}$  soil layer while  $C_{P(k)}$  is the concentration of the total P of the  $k^{th}$  soil layer. As the arbitrary selection of the soil depth may confound the evaluation, three depths (1 m, 2 m and 3 m) were examined for calculating mass proportions of P species for each profile.

#### 2.4. Modified Hedley chemical extractions

We used the modified Hedley methods to extract the operationally-defined pools of P from soils (Hedley et al., 1982; Tiessen and Moir, 1993). Each soil sample was sequentially extracted in duplicate with anion-exchange resin, 0.5 M NaHCO<sub>3</sub>, 0.1 M NaOH, 1 M HCl (hereinafter referred to as "dHCl" for convenience), and concentrated HCl (hereinafter referred to as "cHCl"). The detailed pro-

cedures are provided in EA-3. The residual P after cHCl extraction was determined by the metaborate fusion method (Robertson et al., 1999). Traditionally, the sequential P fractionations assume that dHCl only extracts P<sub>i</sub> (Hedley et al., 1982; Tiessen and Moir, 1993); however, we found it also extracted P<sub>o</sub> (Table A5).

Total P in both dHCl and cHCl extracts was determined by ICP-OES. The NaHCO $_3$  and NaOH extracts were filtered, and aliquots were mixed with ammonium persulfate and then digested in an autoclave at 103.5 kPa and 121 °C to convert all the dissolved P into orthophosphate, which was then measured as total P ( $P_t$ ). We assumed that polyphosphate was negligible in all the extracts, so the  $P_i$  in the extracts was determined using the molybdate blue method (Murphy and Riley, 1962). The  $P_o$  was calculated as the difference ( $P_t$  -  $P_i$ ), and the sum of  $P_o$  in all fractions (i.e., dHCl, NaHCO $_3$ , and NaOH extracts) yielded total  $P_o$ .

The obtained fractions were combined to approximate P pools as follows (Cross and Schlesinger, 1995): Ca–P $_i$  = dHCl–P $_i$ ; non-occluded P (P $_{n-occ}$ ) = resin-P + N aHCO $_3$ –P $_i$  + NaOH–P $_i$ ; occluded P (P $_{occ}$ ) = cHCl–P $_i$  + residual P; and P $_o$  = NaHCO $_3$ –P $_o$  + NaOH–P $_o$  + dHCl–P $_o$  + cHCl–P $_o$ . Similar to the XANES analysis, depthintegrated mass proportions (Eq.8) were also calculated for these P pools.

#### 2.5. Statistical analyses

Pearson correlation analyses were carried out to quantify relationships between key soil chemical properties and P speciation or pools as determined by Hedley extractions and the XANES analyses using SPSS 20. Regression analyses were used to model the data using Origin 2018.

### 3. RESULTS

#### 3.1. Soil properties

The pH of the NE, MID, and SE profiles ranged from 4.8 to 6.9, 5.6 to 6.8, and 3.4 to 5.7, respectively (Fig. 2a-c, Table A3). With increasing depth, the pH decreased to the minimum at B horizons and then increased downward for all three profiles in general. The SOC concentrations were the highest at the surface (111.8 mg/g, 11.7 mg/g, and 41.0 mg/g for NE, MID, and SE profiles, respectively) and monotonically declined with depth, and became very low or non-detectable below the B horizons (Fig. 2d-f, Table A3).

The poorly crystalline Fe (Fe<sub>ox</sub>) concentration in the NE, MID, and SE profiles ranged from 1.0 to 3.5 mg/g, 0.4 to 2.2 mg/g, and 0.2 to 1.9 mg/g, respectively (Fig. 2g-i, Table A3). The Al<sub>ox</sub> concentrations in each profile were comparable to Fe<sub>ox</sub>. The soils in the three profiles contained much more well crystallized Fe oxides (Fe<sub>di</sub>) than Fe<sub>ox</sub>, which ranged from 3.1 to 8.9 mg/g, 3.4 to 16.1 mg/g, and 6.7 to 25.0 mg/g, for the NE, MID, and SE profiles, respectively (Fig. 2j-l, Table A3). However, the Al<sub>di</sub> concentrations were similar to those of Al<sub>ox</sub>. The pedogenic Fe and Al concentrations all reached maxima in the upper B horizons and decreased with depth. DPS<sub>ox</sub> varied from

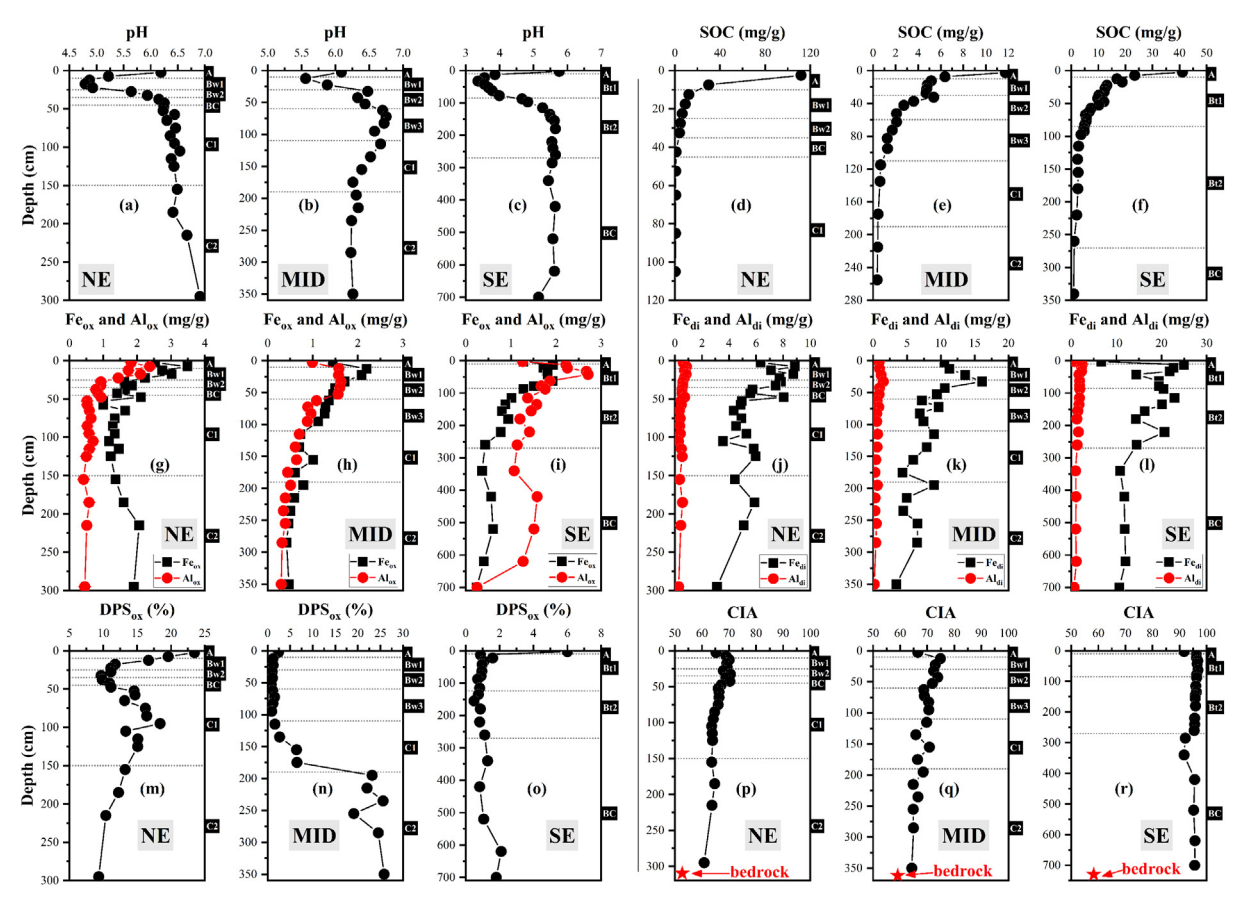


Fig. 2. pH (a, b, c), SOC (d, e, f), oxalate extracted Fe/Al (Fe<sub>ox</sub>, Al<sub>ox</sub>, g, h, i), dithionite extracted Fe/Al (Fe<sub>di</sub>, Al<sub>di</sub>, j, k, l), DPS<sub>ox</sub> (m, n, o), and CIA (p, q, r) as a function of soil depth for the NE, MID, and SE profiles.

9.3% to 23.5%, 0.8% to 25.8%, and 0.5% to 6.0% for the NE, MID, and SE profiles, respectively (Fig. 2m–o, Table A3). A and B horizons of the MID and SE profiles had much lower DPS $_{\rm ox}$  than those of NE (Fig. 2m–o). The three profiles showed the lowest DPS $_{\rm ox}$  in the B horizons, indicating that the poorly crystalline Fe and Al oxides in the B horizons were less saturated with P adsorption than A and C horizons.

The unweathered granite had CIA values of 51.2–59.1 (Fig. 2p–r). The NE profile showed incipient to moderate weathering with the CIA ranging from 60.8 to 70.5 at depths, whereas moderate and extensive weathering occurred to the MID and SE profiles with the CIA values of 65.8–80.9 and 91.7–96.8, respectively (Fig. 2p–r, Table A3). The CIA value increased from the surface to the top B horizons, and then gradually decreased towards the bottom for each profile (Fig. 2p–r).

#### 3.2. Total phosphorus

The total P concentrations in the granite samples collected from the three sites varied substantially from 205 to 841  $\mu$ g/g. The total P concentrations for the NE, MID, and SE profiles were 510–1284  $\mu$ g/g, 99–1104  $\mu$ g/g, and 100–363  $\mu$ g/g, respectively (Fig. 3a–c, Table A3). The  $\tau$ P values calculated with respective to relatively immobile Ti

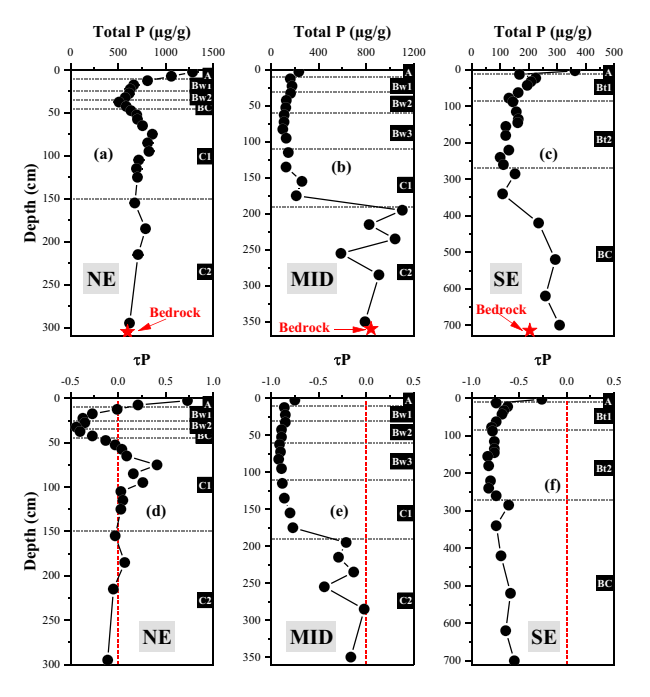


Fig. 3. The total P (a, b, c) and  $\tau_P$  (d, e, f) at different depth for the NE, MID, and SE profiles.

(Eq. (4)) indicated P gains ( $\tau_P > 0$ ) or losses ( $\tau_P < 0$ ) in soil horizons relative to the bedrock (Fig. 3d–f). For the NE profile, the surface soils and the upper part of the C horizons (with the maximal  $\tau_P$  value of 0.73) gained P while the B horizons (with the minimal  $\tau_P$  value of -0.4) lost P (Fig. 3d). Both the MID and SE profiles showed a loss of P at all depths, with  $\tau_P$  values ranging from -0.92 to -0.02 and -0.83 to -0.26, respectively (Fig. 3e, f). The maximal depletion was observed in the B horizons of the MID profile.

The  $\tau_P$  values with depth showed a similar pattern for the NE and MID profiles (Fig. 3d–f). The  $\tau_P$  value decreased from A to B horizons and then increased in the upper part of the C horizons before approaching zero in the lower part of the C horizons. As to the SE profile, for which only A and B horizons were sampled, the  $\tau_P$  value decreased from the surface to the Bt horizons and then slightly increased downward in the BC horizon. This pattern, albeit weaker, was similar to those observed in the A and B horizons of the NE and MID profiles.

#### 3.3. Phosphorus speciation and pools

Phosphorus K-edge XANES analysis was used to characterize the speciation of P<sub>i</sub> in the soil samples based on the type of metal bound to PO<sub>4</sub>. The spectral differences between the samples indicated variations of P speciation with depth in each profile and between the profiles (Fig. A3). In comparison to the P reference spectra shown in Fig. A2, the most prominent features for the NE and MID profiles were that the top horizons had strong (Fe + Al)-P<sub>i</sub> spectral features while the lower part of the C horizons had strong Ca-P; signals. However, the Ca-P; spectral features were barely observed in the SE profile. According to the LCF analysis, the proportion of Ca-P<sub>i</sub> ranged from 0 to 74%, 0 to 47%, and 0 to 16% and (Fe + Al)-P<sub>i</sub> from 26 to 91%, 50 to 72%, and 57 to 89% of total P for the NE, MID, and SE profiles, respectively (Fig. 4a-f). The composition of the P<sub>i</sub> pool showed similar patterns for the NE and MID profiles. Ca-P<sub>i</sub> decreased sharply from the surface (16-17%) to the B horizons (~0%), but increased again until reaching the upper part of the C horizons, and finally gradually increased towards the bottom (24–74%) (Fig. 4a, b), whereas (Fe + Al) $-P_i$ showed an opposite trend as Ca-P<sub>i</sub> with depth (Fig. 4d, e). For the SE profile, Ca-P<sub>i</sub> (16%) was detected only in the surface horizon and (Fe + Al)-P<sub>i</sub> increased with increasing depth (Fig. 4c, f). If only considering the A and B horizons (including BC horizon), all three profiles showed similar patterns of P speciation with depth. If excluding Po, Ca-Pi contributed 0-74%, 0-47%, and 0-22% and (Fe + Al)-P<sub>i</sub> contributed 26-100%, 53-100%, and 78-100% to total inorganic P for the NE, MID, and SE profiles, respectively (data points in red in the Fig. 4af). The proportions of both  $Ca-P_i$  and  $(Fe + Al)-P_i$  over total inorganic P showed similar patterns with depth as

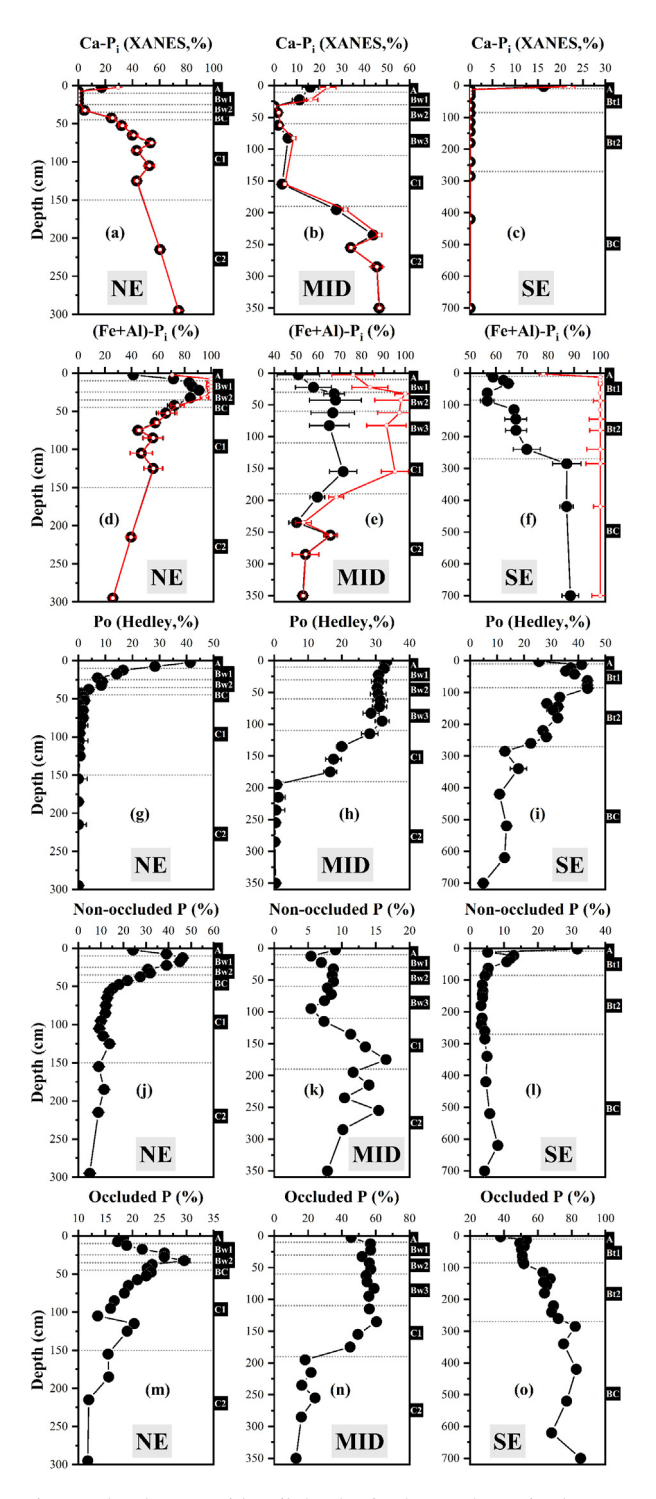


Fig. 4. The changes with soil depth of XANES-determined  $Ca-P_i$  (a, b, c),  $(Fe+Al)-P_i$  (d, e, f), and Hedley-determined  $P_o$  (g, h, i), non-occluded P (j, k, l), and occluded P (m, n, o) for the NE, MID, and SE profiles. The data points in black refer to the percentage over total P, and the points in red in a to f refer to the percentage over total inorganic P.

heir proportions over total P. Note that some samples in the MID and SE profiles had relatively low fitting quality (Fig. A3b, c) as evidenced by the high R-factor values (>0.02, Table A4) because of the noisy spectra due to their low total P concentrations.

To better assess P availability, soil P was fractionated into four pools, i.e., P<sub>n-occ</sub>, P<sub>occ</sub>, dHCl-P and P<sub>o</sub> using the modified Hedley sequential extractions (Fig. 4g-o). P<sub>n-occ</sub>, considered to be biologically available to plants over a short to intermediate term (Martens et al., 1969; Mattingly, 1975; Rowarth and Tillman, 1992; Cross and Schlesinger, 1995), constituted 5.0–46.2%, 5.4–16.5%, and 3.3-31.7% of total P for the NE, MID, and SE profiles, respectively (Fig. 4j–l, Table A5). The P pool with the least availability was Pocc which contributed 11.7-29.6%, 12.9-60.4%, and 38.0-85.3% of total P for the NE, MID, and SE profiles, respectively (Fig. 4m-o). The proportion of Pocc was the highest in the B horizons in each profile. dHCl-P<sub>i</sub>, presumably Ca-P<sub>i</sub>, was dominant in the C but low in A and B horizons, with its proportion ranging from 15.3 - 83.2%, 3.4-79.0%, and 0.2-10.1% of total P for the NE, MID, and SE profiles, respectively (Table A5). However, the extractions overestimated Ca-P<sub>i</sub> for most samples compared to the XANES analysis, despite the existence of a good correlation between the results of the two methods (Fig. A4a). Previous studies also showed that the modified Hedley extractions overestimated Ca-P<sub>i</sub> (Hedley et al., 1982; Benzing and Richardson, 2005; Barrow et al., 2020; Gu et al., 2020), probably because of formation of new Ca-P<sub>i</sub> during alkaline extractions and subsequent removal as Ca-P<sub>i</sub> by dHCl extraction, or dissolution of Fe/Al oxides by dHCl releasing bound P (Barrow et al., 2020; Gu et al., 2020). The extraction-determined P<sub>o</sub> (the sum of NaHCO<sub>3</sub>-P<sub>o</sub>, NaOH-P<sub>o</sub>, dHCl-P<sub>o</sub> and cHCl-P<sub>o</sub>, hereafter referred as P<sub>o</sub>) decreased with increasing depth, with the maximal proportions being 41.3%, 33.0%, and 41.2% of total P for the NE, MID, and SE profiles, respectively (Fig. 4g-i, Table A5). NaOH-P<sub>o</sub> was the largest among the three P<sub>o</sub> fractions.

#### 3.4. Depth-integrated P loss and speciation

From the perspective of the depth-integrated P stock in the entire profile, all three profiles showed a loss of P relative to the bedrock (Fig. 5a), with increasing loss from north to south, also in the order of increasing warmer and wetter climate. Three different depths (1, 2 or 3 m) were chosen for the calculation of depth-integrated mass proportion of P species and pools (Fig. 5b-g). With respect to total P, the proportions of Ca-P<sub>i</sub> and P<sub>n-occ</sub> decreased whereas the proportions of Po and Pocc increased from north to south. The proportion of  $(Fe + Al)-P_i$  over total P increased for the 3-m integration from north to south but decreased for the 1-m integration, whereas it fluctuated for the 2-m depth-integration. However, the proportion of (Fe + Al)-P<sub>i</sub> over total inorganic P increased from north to south for all three depth integrations (Fig. A5). The greater P<sub>o</sub> inputs in topsoil in the warm and humid sites also result in a reduction of the percentage of (Fe + Al) $-P_i$  in total P, concealing the increasing trend of the (Fe + Al)-P<sub>i</sub> proportion over total P during 1-m and 2-m depth-integrated calculations. In addition, as the integration soil thickness increased from 1 m to 3 m, Ca–P $_{\rm i}$  contributed more and both P $_{\rm o}$  and P $_{\rm n\text{-}occ}$  contributed less to the total P for each profile; the proportions of (Fe + Al)–P $_{\rm i}$  and P $_{\rm occ}$  decreased for the NE and MID profiles but increased for the SE profile.

We also evaluated the influence of denudation rate, slope, and SRT on P loss and P speciation at the profile level (Fig. 5h-j). Given that the shallow soil thicknesses used in the depth-integrated calculation could overemphasize the contribution of surface soils into the P stock and speciation in a soil profile, here we used the 3-m depth-integrated mass proportion of P species and the depth-integrated P loss percentage of entire profile to compare the influences of the three factors. The results showed that depth-integrated P loss and speciation fluctuated with increasing denudation rate, slope, or SRT (Fig. 5h-j).

# 3.5. Correlations of soil P pool and speciation with edaphic variables

To understand how soil properties affect P speciation and pool, we further explored the correlations between the edaphic variables and the P speciation and pools determined from the modified Hedley extractions and XANES spectroscopy by compiling the data from all soil samples into one dataset regardless of climate and soil depth (Fig. 6, Table A6). The proportion of Ca-P<sub>i</sub> over total P correlated positively with soil pH, while the proportions of (Fe + Al)-P<sub>i</sub>, P<sub>o</sub>, and P<sub>occ</sub> over total P correlated negatively with soil pH (Fig. 6a, b, e, g). After excluding Po, the correlation between pH and the proportion of Ca-P<sub>i</sub> or (Fe + Al)-P<sub>i</sub> over total P<sub>i</sub> became stronger (Fig. 6c, d). Interestingly, at pH < 5.5, (Fe + Al)- $P_i$  was the only  $P_i$  species, whereas at pH from 5.5 to 7, the proportions of (Fe + Al)-P<sub>i</sub> and Ca-P<sub>i</sub> over total P<sub>i</sub> followed a strong linear relationship with pH if we excluded a cluster of data points (green points in the black circles in the Fig. 6c, d) from the MID profile. These outliers were probably ascribed to the unreliable LCF analysis caused by the relatively high noise levels of the spectra of these samples (Fig. A3b). The regression equation predicts that Ca-P<sub>i</sub> was the only  $P_i$  species at pH > 7.4.

As to the correlations with pedogenic Fe and Al oxides, the  $P_{\rm occ}$  proportion over total P correlated positively with both Fe\_{di} and Al\_{di} concentrations, the (Fe + Al)–P\_i proportion over total P with Al\_{ox} concentration (Table A6), and the P\_o concentration with both SOC and Fe\_{ox} + Al\_{ox} concentration (Fig. 6h, i). The proportion of (Fe + Al)–P\_o as calculated using Eq. (6) was found to correlate with the Fe\_{ox} + Al\_{ox} concentration (Fig. 6k).

In addition, we determined the correlations between CIA and the P speciation and pools. The proportions of Ca– $P_i$  and  $P_{n\text{-}occ}$  over total P correlated negatively with CIA whereas the proportions of (Fe + Al)– $P_i$ ,  $P_o$  and  $P_{occ}$  over total P correlated positively with CIA (Fig. 7a, b, e, f, g). If excluding  $P_o$  (i.e., over total  $P_i$ ), the correlation between CIA and the (Fe + Al)– $P_i$  proportion became stronger (Fig. 7d).

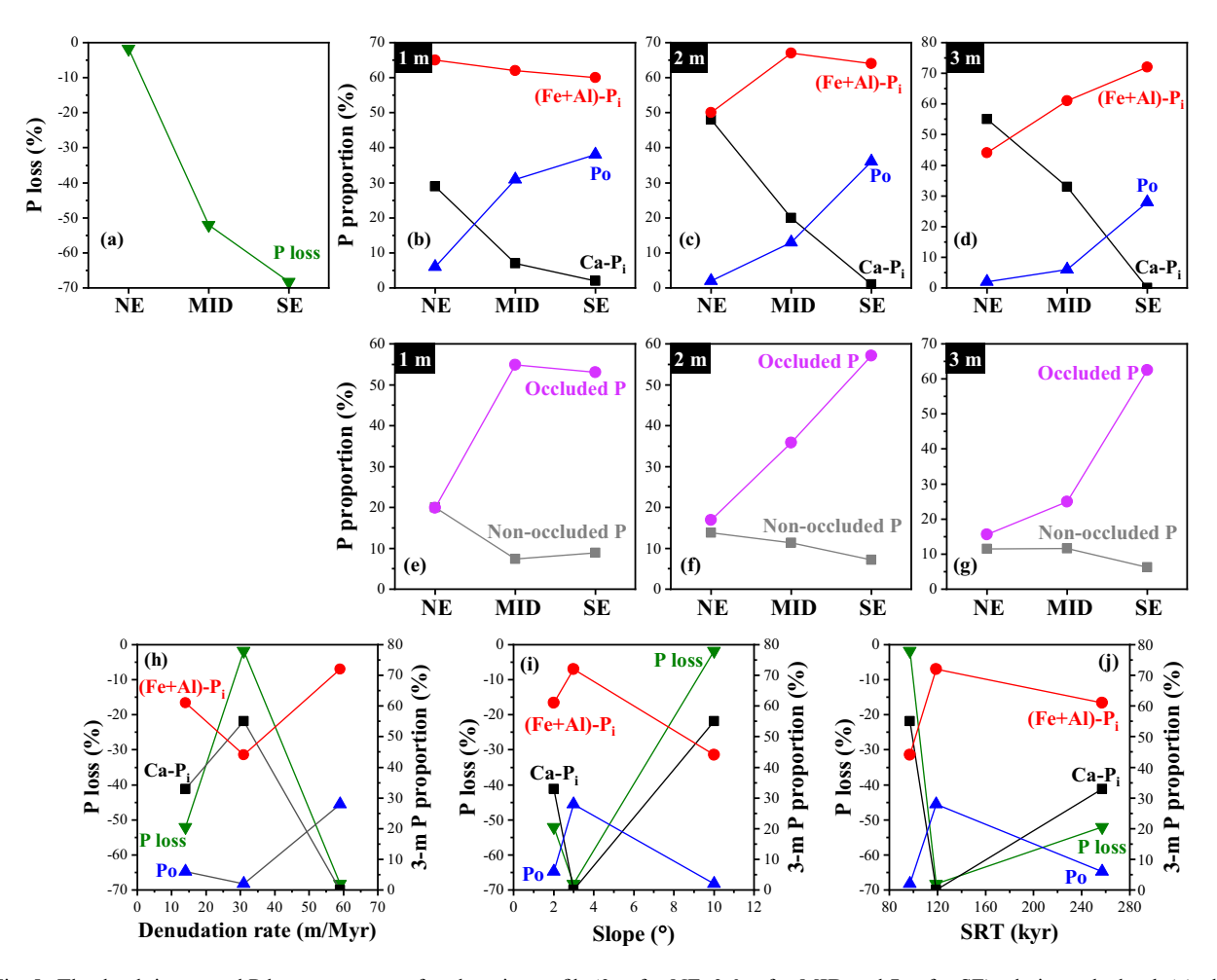


Fig. 5. The depth-integrated P loss percentage of each entire profile (3 m for NE, 3.6 m for MID and 7 m for SE) relative to bedrock (a); the depth-integrated mass proportion of  $Ca-P_i$ , (Fe + Al)- $P_i$  and  $P_o$  over total P for 1 m (b), 2 m (c) and 3 m (d), respectively; the depth-integrated mass proportion of non-occluded and occluded P over total P for 1 m (e), 2 m (f) and 3 m (g), respectively; and the depth-integrated P loss and speciation (3 m) versus denudation rate (h), slope (i), and soil residence time (SRT, j).

#### 4. DISCUSSION

# 4.1. Effects of climate on P loss and speciation at the whole profile level

Given that the three studied soil profiles differ in climate, tectonics, topography, and pedogenic time, we first evaluate the influence of these four factors on P loss and P speciation. The denudation rates, slopes, and SRT of profiles can be used as the proxy of tectonics, topography, and pedogenic time of profile, respectively (Riebe et al., 2001; Dixon et al., 2012; Heimsath et al., 2012; Dere, 2014; Riebe et al., 2017). High denudation rate and steep slope increase P loss (Aciego et al., 2017; Arvin et al., 2017), while the duration of pedogenesis significantly alters P stock and speciation by decreasing total P concentration and the Ca-P<sub>i</sub> proportion and increasing the proportions of (Fe + Al)-P<sub>i</sub> and P<sub>o</sub> as described in the Walker and Syers (1976) model. However, our results show that the depthintegrated P loss and speciation do not monotonically vary with increasing denudation rate, slope, or SRT (Fig. 5d–f),

suggesting that the tectonics, topography, and SRT are not the major factors influencing P concentration and speciation in these profiles. In contrast, both P loss and speciation display a monotonically increasing or decreasing trend as the climate becomes warmer/wetter (Fig. 5a, d). In addition, dust deposition can also affect soil P stock and speciation (Crews et al., 1995; Eger et al., 2013; Aciego et al., 2017; Gu et al., 2019; Gallardo et al., 2020). However, climate strongly affects the magnitude of dust influence on P concentration, speciation and availability in soils (Gu et al., 2019). The influence is stronger in colder/drier climate with weak weathering, such as for the NE site, but weaker in warmer/wetter climate, such as for the MID and SE sites due to intense weathering and rapid alteration of dust materials (Gu et al., 2019). Overall, the observations in the present study can be largely understood by considering climate as the primary controlling factor, although the three sites do not form a well-constrained climosequence as well as receive aeolian dust inputs.

The warmer/wetter climate as at the SE site leads to the faster depletion of P compared to the colder/drier climate

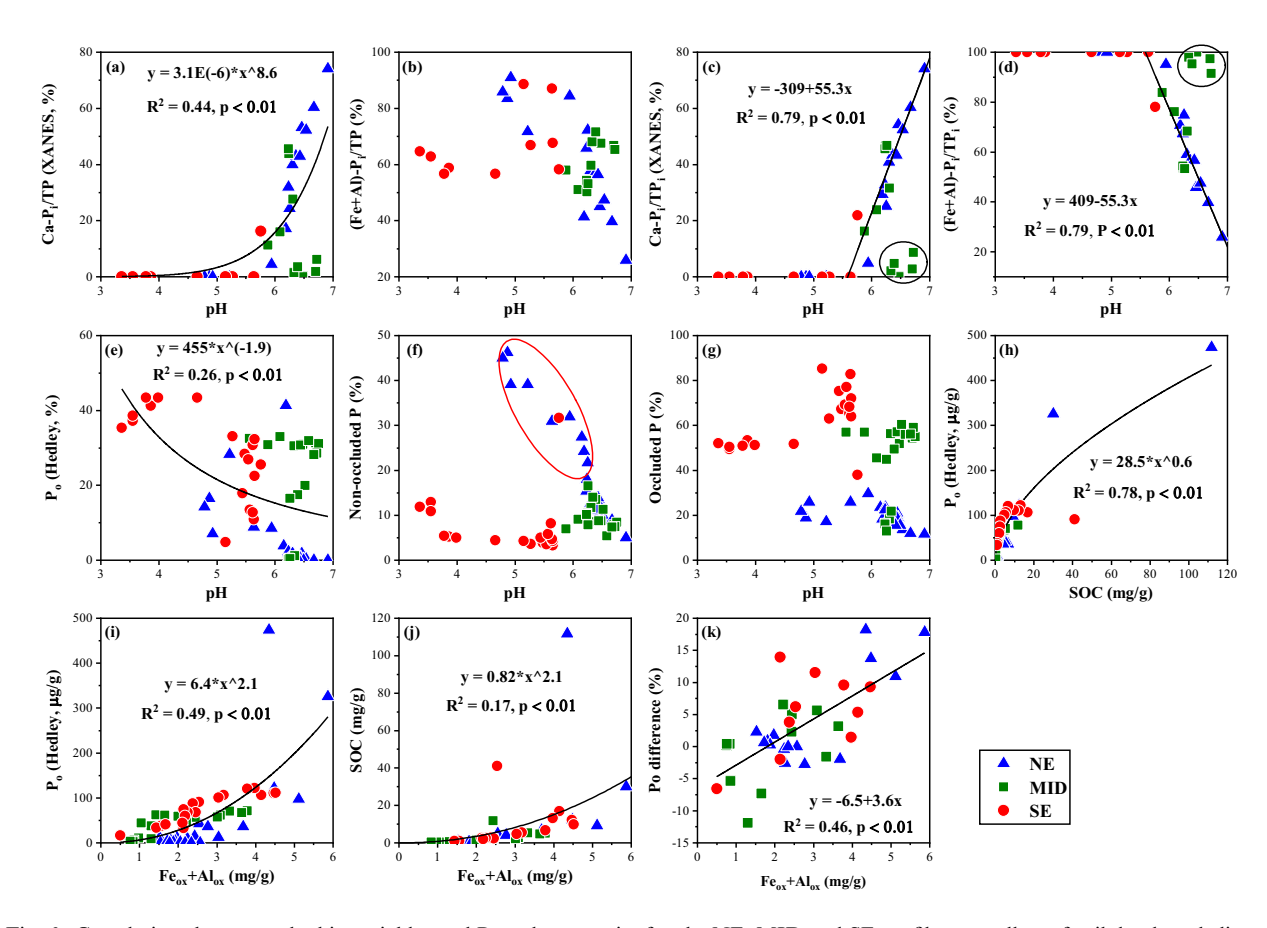


Fig. 6. Correlations between edaphic variables and P pools or species for the NE, MID and SE profiles regardless of soil depth and climate. The percentage in (a, b, e, f, g) is relative to total P. The percentage in (c and d) is relative to the total inorganic P.  $P_0$  difference in (k) refers to the difference between the extraction- and XANES-determined  $P_0$  proportions (Eq. (6)). The data points in the black circles in c and d are excluded from the regression analyses, while other regression curves are obtained from all the data.

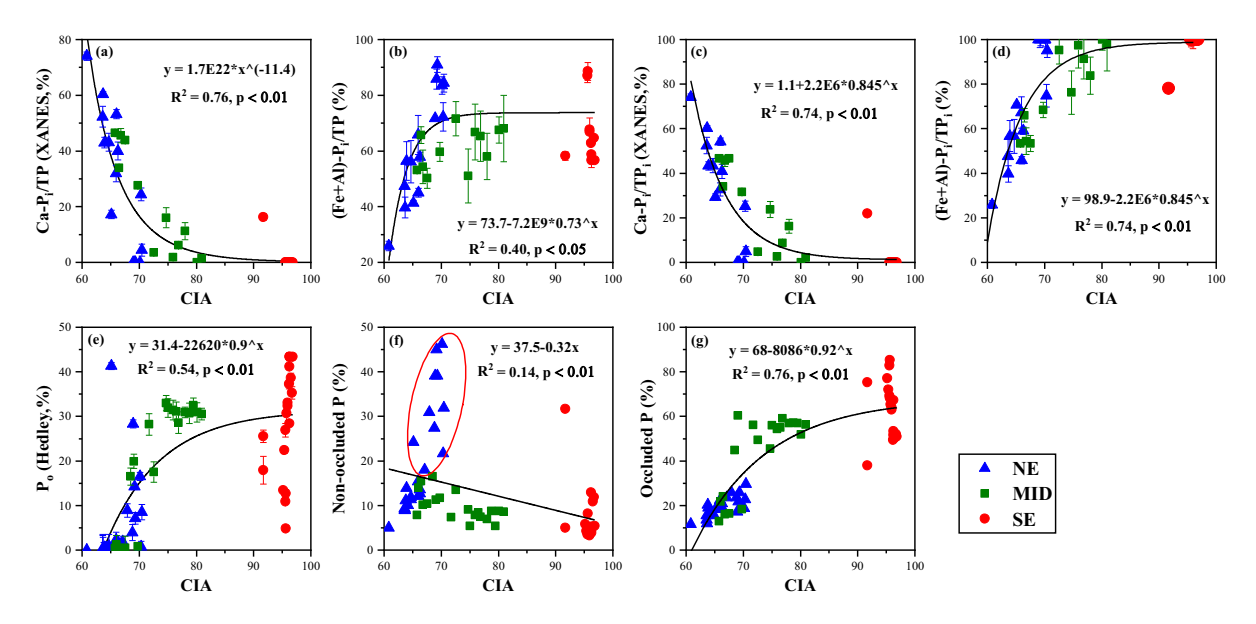


Fig. 7. Correlations between chemical index of alteration (CIA) and the percentage of each P pools or species relative to total P (a, b, e, f, g), and between CIA and the percentage of each inorganic P species over the total inorganic P (c, d) for the NE, MID, and SE profiles. All data points shown in each plot were used for the regression analyses.

as at the NE and MID sites due to the stronger weathering and leaching in the warmer/wetter climate (Fig. 5a). Accordingly, little Ca–P<sub>i</sub> is found in the SE profile (Figs. 5b–d and 4c), consistent with the soils of similar age in the tropical forests in New Zealand and Hawaii where Ca–P<sub>i</sub> is exhausted after approximately 10,000 years of pedogenesis (Walker and Syers, 1976; Crews et al., 1995). (Fe + Al)–P<sub>i</sub> gradually increases as the climate becomes warmer/wetter (Fig. 5d), consistent with increasing weathering degree (Fig. 2p–r). Meanwhile, a larger proportion of P<sub>o</sub> is associated with increasing biomass production and greater P inputs as organic residues as the climate becomes warmer/wetter (Cross and Schlesinger, 2001).

#### 4.2. Vertical distribution of P concentration and speciation

Our results show that the P concentration and speciation in each soil profile do not change monotonically with soil depth (Figs. 3 and 4) because the profile undergoes stratification of soil properties with depth (Fig. 2) due to pedogenesis. Moreover, the three soil profiles by large follow similar P vertical distribution and speciation patterns, although climatic conditions and other soil formation factors affect P speciation and the magnitude of the P loss (Fig. 5). The similarity can be ascribed to that all the profiles are shaped by the same set of pedogenic processes. However, soil formation factors, such as climate, affect the intensities of these processes and thus the details of the P concentration and speciation patterns (Figs. 3 and 4).

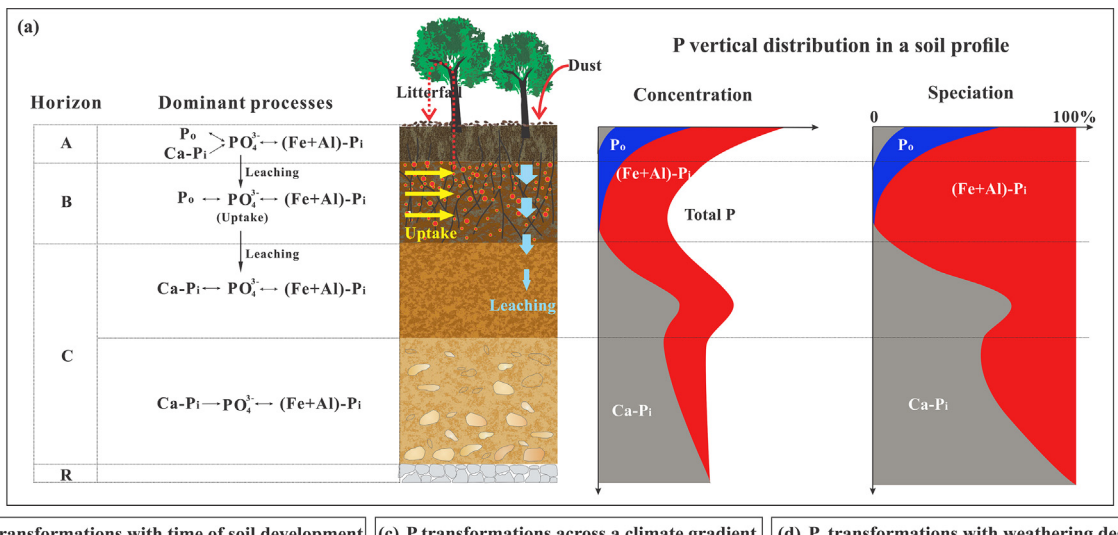
Based on the results, we propose a one-dimensional conceptual model to describe the P vertical distribution and speciation patterns that are shaped by chemical weathering, aeolian dust inputs, leaching and biolifting (Fig. 8a). The conceptual model is summarized as (i) an upward increase in total P, Ca-P<sub>i</sub> and P<sub>o</sub> in the A horizons due to biolifting and dust inputs, (ii) P depletion in the B horizons caused by the strong weathering, plant uptake and leaching removal with the remaining P primarily in the (Fe + Al)-P<sub>i</sub> form, (iii) an increase in total P concentration in the upper part of the C horizons with most P in the form of Ca-Pi likely due to limited leaching and neoformation of Ca-Pi, and (iv) a downward increase in Ca-P<sub>i</sub> and decrease in (Fe + Al)-P<sub>i</sub> in the lower part of the C horizons due to chemical weathering and negligible P loss or gain. In the following, we discuss the patterns and the associated processes in details for each horizon.

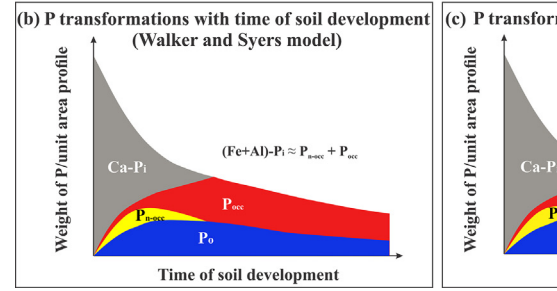
As for A horizons, the relatively high total P, Ca–P<sub>i</sub> and P<sub>o</sub> concentrations (Figs. 3, 4a–c, and g–i) compared to the underneath B horizons can be attributed to both biolifting of P from the B horizons (Scholes and Archer, 1997; McCulley et al., 2004; Sardans and Peñuelas, 2014; Bullen and Chadwick, 2015, 2016) and aeolian dust inputs (Derry and Chadwick, 2007; Aciego et al., 2017). Both dust and P<sub>o</sub> accruals become weaker with increasing depth. P<sub>o</sub> accounts for large proportions (25–41%) in the A horizons (Fig. 4g–i) in parallel with the accumulation of soil organic matter (SOM) there (Fig. 2d–f), indicating the importance of biolifting in increasing total P concentration in the A horizons (Jobbágy and Jackson, 2001). The presence of significant Ca–P<sub>i</sub> (16–17%) in surface soils of all three profiles

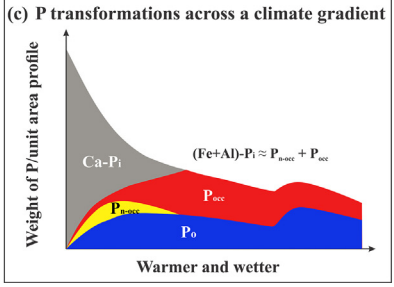
suggests aeolian dust inputs. The continental dust from central Asia contains abundant Ca-P<sub>i</sub> (Chen et al., 2006; Flaum, 2008). It is rich in carbonates and poorly weathered materials (Shen et al., 2007; Gu et al., 2019), and thus can neutralize soil acidity, particularly for the surface soils, and increase the stability of Ca-Pi compounds (Shen et al., 2007; Gu et al., 2019). Dust inputs are particularly important for the NE profile having a net gain of P near the soil surface with a  $\tau_P$  value up to 0.73 (Fig. 3d). The average P in the Asian aeolian dust from Chinese Loess Plateau is about 1146 µg/g (Flaum, 2008; Ni et al., 2015), 1.9 times higher than the P concentration in the granitic bedrock of the NE site. Thus, it is not surprising that dust deposition will increase the total P concentration above the bedrock value for the surface soils of the NE profile. Although the MID and SE profiles receive dust inputs as well (Li et al., 2016), the warmer/wetter climate results in rapid dissolution of dust and leaching, thus only slight increases in total P concentration at surface (Fig. 3e, f).

The total P depletion in the B horizons is the strongest among all layers (Fig. 3), and the P speciation therein is dominated by (Fe + Al) $-P_i$  (58–91%) with little Ca $-P_i$  (0– 6%) (Fig. 4a-f). All these observations can be attributed to the strong weathering (i.e., the highest CIA values), biolifting and downward leaching in the B horizons. Organic acids, such as oxalic and citric acids, produced by plant roots, microorganisms and fungi are generally more abundant in B horizons than in A horizons (Fox and Comerford, 1990), which enhances weathering and Ca-P<sub>i</sub> dissolution (Welch et al., 2002; Goyne et al., 2006). Organic acids can also compete with phosphate to bind to mineral surfaces, jeopardizing P sorption and thus promoting plant uptake and leaching of soluble P. Previous studies also found low Ca-P<sub>i</sub> in acidic B horizons (pH 4.9-5.5) (Ippolito et al., 2010; Amelung et al., 2015) but not as low as our results, probably because previous studies used chemical extractions that might overestimate Ca-P<sub>i</sub> (Barrow et al., 2020; Gu et al., 2020). While the MID profile is developed under intermediate climatic conditions, it has the largest P loss in B horizon among the three profiles, which can be ascribed to its longest soil residence time among the three profiles.

The C horizons are influenced little by biological activities, as indicated by the low SOC and Po concentrations (Figs. 2d-e, and 4g-i). The chemical weathering is weak, and the weathering degree decreases with increasing depth throughout the entire C horizons of both NE and MID profiles (Fig. 2p-r). Leaching loss of P is essentially negligible as indicated by the constant total P concentration in the lower part of the C horizons for the NE and MID profiles (Fig. 3d, e). Vertical material transport occurs substantially only to the upper part of the C horizons. An increase in total P in the upper part of the C horizons (Fig. 3d) is largely attributed to a sharp decrease in permeability there. Similar phenomenon was observed previously for Ca<sup>2+</sup> and SO<sub>4</sub><sup>2</sup> that increased down profiles and re-precipitated as CaSO<sub>4</sub> at impermeable soil-bedrock interface (Rea et al., 2020). The XANES results show that the accumulated P is composed of largely Ca-P<sub>i</sub> (Fig. 4a), suggesting that a portion of the Ca-P<sub>i</sub> may be newly formed from







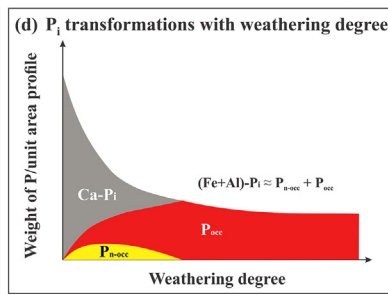


Fig. 8. (a) The dominant biogeochemical and physical processes pertinent to P in each soil horizon of the forest soil profiles and the schematic illustrations of the vertical distribution patterns of P concentration and speciation. (b) Phosphorus transformations with time of soil development as described in the Walker and Syers model. (c) Phosphorus transformations across a climate gradient. (d) Inorganic P species (P<sub>i</sub>) transformations with weathering degree, such as CIA.

 $\text{Ca}^{2+}$  and phosphate accumulated there. The slightly acidic pH of the soils (6.2–6.5) might not prevent the formation of  $\text{Ca-P}_i$ , as Weng et al. (2011) showed that  $\text{Ca-P}_i$  can be stable at pH  $\sim$  6.5. Compared to the NE profile, the weaker P accumulation in the upper part of the C horizon of the MID profile is consistent with its stronger P loss under the warmer/wetter climate (Fig. 3e). While the total P concentration varies little with depth due to limited P loss or input in the lower part of the C horizons (Fig. 3d, e), the  $\text{Ca-P}_i$  proportion decreases and the (Fe + Al)–P<sub>i</sub> proportion increases with decreasing depth (Fig. 4a, b, d, e), consistent with the increasing weathering degree.

#### 4.3. Vertical distribution of phosphorus availability

Phosphorus speciation and concentration in turn affect P availability at depth. The proportion of P<sub>occ</sub>, which is mostly associated with pedogenic Al and Fe minerals, shows similar trends to (Fe + Al)–P<sub>i</sub> (Fig. 4d–f), reaching the maximum values in the B horizons of the NE profile but also becoming the dominant P pool in the B horizons of both MID and SE profiles (Fig. 4m–o). Previous studies have shown considerable potentials for nutrient acquisition from B horizons by deep-rooting plants for forest ecosystems (Scholes and Archer, 1997; McCulley et al., 2004; Sardans and Peñuelas, 2014; Bullen and Chadwick, 2015, 2016). However, the depletion of Ca–P<sub>i</sub> and dominance of P<sub>occ</sub> in the B horizons result in low P availability, which

may limit the growth of forests. The proportion of  $P_{\rm occ}$  increases from north to south (Fig. 4m–o, 5e–g), consistent with the greater production of pedogenic Fe and Al minerals in the warmer/wetter climate (Fig. 2j–l).

No consistent pattern with depth is observed for P<sub>n-occ</sub> for the three soil profiles (Fig. 4j-1), which is likely because  $P_{n-occ}$  is sensitive to the influence of multiple factors, such as dust inputs, leaching, biological activities, and pedogenic Fe and Al minerals. As to the NE profile, the large proportions of P<sub>n-occ</sub> (21.7-46.2%) in the A and B horizons (Fig. 4j) could be caused by dissolution of dust-borne Ca-P<sub>i</sub> in the acidic soil layers (Crews et al., 1995; Eger et al., 2013; Gu et al., 2019). However, the MID and SE profiles have low proportions of  $P_{n-occ}$  (Fig. 4k, 1). Although the MID and SE profiles receive dust inputs as well (Li et al., 2016), the warmer/wetter climate results in high phosphate fixation and strong leaching of P<sub>n-occ</sub>, thus low P<sub>n-occ</sub>. Moreover, although increasing Po mineralization (Walker and Syers, 1976; Crews et al., 1995; Izquierdo et al., 2013) and reducing environments can increase P<sub>n-occ</sub> (Miller et al., 2001; Chacon et al., 2006; Liptzin and Silver, 2009) at the warmer/wetter sites as in MID and SE, increasing precipitation also promotes leaching of P<sub>n-occ</sub>. Meanwhile, the MID and SE profiles have higher concentrations of pedogenic Fe and Al minerals (Fig. 2j-1), which are effective sorbents for phosphate to produce Pocc (Parfitt, 1989). Consistently, DPSox values demonstrate a much lower saturation of adsorbing sesquioxides surfaces with P in the A

and B horizons for the MID and SE profiles compared to the NE profile (Fig. 2m-o), resulting in a lower risk of P mobilization by P desorption from sesquioxides of the former two profiles.

# 4.4. Controls of edaphic variables on soil P pools and speciation

The correlation analyses indicate that both CIA and pH (Figs. 6a-d and 7a-d) can be used to predict the speciation of the P<sub>i</sub> pool regardless of climate and soil depth, indicating that the P<sub>i</sub> speciation is primarily controlled by soil geochemistry and mineralogy. The correlations with pH suggest that all Ca-P<sub>i</sub> is exhausted at pH < 5.5, and (Fe + Al)- $P_i$  is not produced at pH > 7.4 (Fig. 6c, d); and their proportions over total P<sub>i</sub> change linearly between the two pH thresholds. The correlation with pH is consistent with the laboratory experiments showing that all Ca-P<sub>i</sub> in soils were dissolved at pH 5.5 (Andersson et al., 2016). The P<sub>i</sub> speciation-pH correlation suggests that P speciation, i.e., the relative proportions of  $Ca-P_i$ ,  $(Fe + Al)-P_i$ , and P<sub>o</sub> over total soil P, can be approximately estimated by measuring soil pH, and Po and total P concentrations without a need to conduct an X-ray absorption spectroscopic analysis.

The proportion of  $P_{\rm occ}$  over total P correlates well with CIA (Fig. 7g) but not with pH (Fig. 6g), attributed to that CIA reflects not only soil geochemistry but also mineralogy. In other words, soil mineralogical composition strongly affects P occlusion by minerals in addition to soil pH. The proportion of  $P_{\rm n-occ}$  over total P correlates weakly with CIA (Fig. 7f) and not with pH (Fig. 6f). The A and B horizons of the NE profile and the A horizon of the SE profile (i.e., the data points in the red circles in the Fig. 7f) deviate from the expected trend line between  $P_{\rm n-occ}$  and CIA. The deviation is consistent with that the vertical distribution of  $P_{\rm n-occ}$  in soils is poorly constrained because it is sensitive to influence of many factors as discussed above.

Organic P concentration correlates well with SOC content (Fig. 6h) but weakly with CIA (Fig. 7e) and pH (Fig. 6e) because biological processes largely determine P<sub>o</sub> production and consumption. The correlation with SOC (Fig. 6h) indicates coupling of SOC and Po in soils (Tipping et al., 2016; Spohn, 2020). Po concentration also correlates to some extent with Fe<sub>ox</sub> + Al<sub>ox</sub> concentration (Fig. 6i), suggesting that some P<sub>o</sub> compounds are associated with poorly crystalline Fe and Al. Most Po in soils are phosphate esters that contain the PO<sub>4</sub> moiety. These P<sub>o</sub> esters, particularly monoesters, can bind to Fe/Al via PO<sub>4</sub> (Wang et al., 2017). Up to 18% of total P<sub>o</sub> is estimated to bind to Fe/Al in our soil samples (Eq. (6)) and the portion of Po correlates well with the oxalate-extracted Fe and Al content (Fig. 6k). The adsorption by pedogenic Fe and Al minerals can contribute to the long-term persistence of P<sub>o</sub> in soils as it does for SOM (Cotrufo et al., 2013). Some of the Po compounds are associated with SOM but do not bind to Fe and Al. An important portion of such SOM can be particulate organic matter (POM) with low decomposition degrees. These Po can be protected by minerals as well from enzymatic mineralization if the POM is physically inaccessible to enzymes and microbes due to encapsulation within microaggregates (Golchin et al., 1997). Apparently,  $P_o$  is better protected by mineral sorption than by association to POM. Overall, the  $P_o$  concentration in soils is controlled by both biological activities and geochemistry/mineralogy.

These identified strong correlations between P speciation and the edaphic variables are obtained from the soils varying greatly in soil properties since they were collected at different depths under contrasting climate. Thus, the obtained correlations may apply to a wide variety of soils in diverse ecosystems.

# 4.5. Use of environmental gradients for studying phosphorus transformations during pedogenesis

Soil P transformations during pedogenesis have been assessed mainly with soil chronosequences (i.e., comprising soils of increasing pedogenic times) based on depthintegrated stock of various P pools operationally defined by sequential chemical extractions (Walker and Syers, 1976; Crews et al., 1995; Prietzel et al., 2013; Chen et al., 2015). Empirical evidence leads to the development of the conceptual Walker and Svers model (Fig. 8b) that describes P transformations with soil development. In the Walker and Syers model, primary P minerals weather and release soluble P to soil solution. The soluble P is lost via leaching and runoff, assimilated by biota to form Po, or adsorbed/precipitated on the surface of secondary Fe and Al minerals, giving rise to Po, Pn-occ and Pocc at early stage of soil development. After an intermediate stage of soil development with optimal P supply and maximum diversity of P species, a small fraction of the initial soil P is stored organically or occluded in Fe/Al oxyhydroxides, thus becoming unavailable to plants and microorganisms (Walker and Syers, 1976; Crews et al., 1995; Prietzel et al., 2013; Turner and Laliberté, 2015).

Weathering profiles may also be used for studying P transformations during soil development, as suggested by Mishra et al. (2013) and Newman et al. (2020). However, our results show that none of the vertical patterns of P concentration, speciation and availability follow the Walker and Syers model (Figs. 3 and 4). This is primarily because the vertical material transport, dust inputs, and rhizosphere processes in root zones result in stratification of soil properties with depth, particularly in the upper soil horizons, preventing its use for studying P transformations during pedogenesis. Only the P<sub>i</sub> speciation pattern in the bottom part of the profile (i.e., the lower part of the C horizons) is analogous to that described in the Walker and Svers model (Fig. 8a). Nonetheless, the nearly constant total P concentration and little Po present there are inconsistent with the accumulation of Po and loss of total P during pedogenesis.

Climosequences have potentials to be used for studying P transformations during soil development as well (Hou et al., 2018). Consistent with the present study (Fig. 5), previous studies showed that climatic conditions with MAP less than 2750 mm followed the Walker and Syers model during pedogenesis (Fig. 8c) (Miller et al., 2001; Ippolito

et al., 2010; Emadi et al., 2012; Feng et al., 2016; Deiss et al., 2018; Hou et al., 2018). However, MAP greater than 2750 mm can lead to anaerobically driven accumulation of P<sub>o</sub> in volcanic soils, which can offset the loss of recalcitrant (Fe + Al)-P<sub>i</sub> due to reduction of Fe oxides and thus produce a non-linear increase in total P (Miller et al., 2001) (Fig. 8c). This suggests that climosequences across a certain MAP range can be used to study P transformations. However, it is challenging to find sites of climosequences with similar vegetation type as vegetation often co-varies with climate, and the variation in the vegetation type could confound the results.

Phosphorus transformations may be studied using weathering degree as the variable, such as CIA, regardless of the state factors of soil formation. Both  $P_i$  speciation and  $P_{\rm occ}$  have strong correlations with CIA regardless of soil depth and climate (Fig. 7c, d, g). However, both  $P_o$  and  $P_{\rm n-occ}$  have weak correlations with CIA (Fig. 7e, f). Thus, similar to the lower part of the C horizons, CIA may be used to evaluate the transformations of  $P_i$ , but not for  $P_o$ , during pedogenesis (Fig. 8d).

#### 5. CONCLUSIONS

A combination of the use of fine-scale soil sampling intervals and spectroscopic and extraction analyses allows for identifying detailed vertical distribution patterns of P concentration, speciation and availability. The major features of the patterns under three climate conditions are similar and can be well understood by considering the relative importance of several pedogenic processes. A onedimensional conceptual model is proposed to describe the patterns and related processes, which provides a framework for understanding how pedogenesis redistributes and transforms P in soil profiles. The experimental data and the model can be useful for future development of reactive transport models to predict the transformations and transport of P during pedogenesis. We further found that Po and SOC were coupled and an important portion of Po was stabilized by poorly crystalline Fe and Al, suggesting a possible role of mineralorganic matter association in stabilizing Po as for SOC, which needs to be further studied. Future studies are also warranted to confirm or refine the quantitative relationships between those edaphic variables (pH, CIA, SOC, and pedogenic Fe and Al) and P speciation using more diverse ecosystems varying in the state factors of soil formation. Such quantitative relationships could be useful to understand soil P speciation and availability in a global context. Soil climosequences, weathering profiles and CIA gradients provide rich information about P transformations during pedogenesis while they may have more constraints than soil chronosequences for studying P transformations. Overall, this study improves the current understanding of how climatic and edaphic variables influence P dynamics in soil profiles, which is useful to predict responses of P availability in soils to global climate change.

#### **Declaration of Competing Interest**

The authors declare that they have no known competing financial interests or personal relationships that could have appeared to influence the work reported in this paper.

#### **ACKNOWLEDGEMENTS**

This work was funded by U.S. National Science Foundation Faculty Early Career Development Program (EAR-1752903). Partial support was from the Roy J. Shlemon Center for Quaternary Studies at the University of Wyoming. Z. Zhang also thanks the support from the Chinese Scholarship Council. C. Liu and Z. Zhao thank the support from the National Natural Science Foundation of China (Grant Nos. 41930863, 41661144042, 41130536). C. Liang is grateful to the support from National Key R&D Program of China (No. 201YFD0800103). We thank T. Liu, L. Cui, B. Fan, and H. Mao for collecting the soil samples used in this study. The authors are grateful to Ph.D. student Ms. Than Dam in Soil and Environmental Biogeochemistry Group at the University of Wyoming for her assistance in identifying soil horizons. Canadian Light Source is supported by the Natural Sciences and Engineering Research Council of Canada, the National Research Council Canada, the Canadian Institutes of Health Research, the Province of Saskatchewan, Western Economic Diversification Canada, and the University of Saskatchewan.

#### APPENDIX A. SUPPLEMENTARY MATERIAL

Supplementary data to this article can be found online at https://doi.org/10.1016/j.gca.2021.07.002.

### REFERENCES

Aciego S. M., Riebe C. S., Hart S. C., Blakowski M. A., Carey C. J., Aarons S. M., Dove N. C., Botthoff J. K., Sims K. W. W. and Aronson E. L. (2017) Dust outpaces bedrock in nutrient supply to montane forest ecosystems. *Nat. Commun.* 8, 14800.

Amelung W., Antar P., Kleeberg I., Oelmann Y., Lücke A., Alt F., Lewandowski H., Pätzold S. and Barej J. A. M. (2015) The δ18O signatures of HCl-extractable soil phosphates: methodological challenges and evidence of the cycling of biological P in arable soil. *Eur. J. Soil Sci.* **66**, 965–972.

Anderson S. P., Dietrich W. E. and Brimhall G. H. (2002) Weathering profiles, mass-balance analysis, and rates of solute loss: Linkages between weathering and erosion in a small, steep catchment. *Geol. Soc. Am. Bull.* **114**, 1143–1158.

Andersson K. O., Tighe M. K., Guppy C. N., Milham P. J., McLaren T. I., Schefe C. R. and Lombi E. (2016) XANES demonstrates the release of calcium phosphates from alkaline Vertisols to moderately acidified solution. *Environ. Sci. Technol.* 50, 4229–4237.

Arvin L. J., Riebe C. S., Aciego S. M. and Blakowski M. A. (2017) Global patterns of dust and bedrock nutrient supply to montane ecosystems. Sci. Adv. 3, eaao1588.

Barrow N. J., Sen A., Roy N. and Debnath A. (2020) The soil phosphate fractionation fallacy. *Plant. Soil.*, 1–11.

Baumann K., Shaheen S. M., Hu Y., Gros P., Heilmann E., Morshedizad M., Wang J., Wang S.-L., Rinklebe J. and Leinweber P. (2020) Speciation and sorption of phosphorus in

- agricultural soil profiles of redoximorphic character. *Environ. Geochem. Health.* 1–16.
- Beauchemin S., Hesterberg D., Chou J., Beauchemin M., Simard R. R. and Sayers D. E. (2003) Speciation of phosphorus in phosphorus-enriched agricultural soils using X-ray absorption near-edge structure spectroscopy and chemical fractionation. *J. Environ. Qual.* 32, 1809–1819.
- Benzing P. and Richardson C. J. (2005) CaCO3 causes underestimation of NaOH extractable phosphorus in sequential fractionations. *Soil Sci.* 170, 802–809.
- Blake G. R. and Hartge K. H. (1986) Bulk density. In *Methods of Soil Analysis: Part 1. Physical and Mineralogical Methods* (ed. A. Klute). Soil Science Society of America, Madison, pp. 363–382.
- Brantley S. L. and Lebedeva M. (2011) Learning to read the chemistry of regolith to understand the Critical Zone. *Annu. Rev. Earth Planet. Sci.* **39**, 387–416.
- Brimhall G. H. and Dietrich W. E. (1987) Constitutive mass balance relations between chemical-composition, volume, density, porosity, and strain in metasomatic hydrochemical systems Results on weathering and pedogenesis. *Geochim. Cosmochim. Acta* 51, 567–587.
- Bullen T. and Chadwick O. (2015) Evidence for nutrient biolifting in Hawaiian climosequence soils as revealed by alkaline earth metal stable isotope systematics. *Procedia Earth Planet. Sci.* 13, 312–315.
- Bullen T. and Chadwick O. (2016) Ca, Sr and Ba stable isotopes reveal the fate of soil nutrients along a tropical climosequence in Hawaii. *Chem. Geol.* **422**, 25–45.
- Buss H. L., Chapela Lara M., Moore O. W., Kurtz A. C., Schulz M. S. and White A. F. (2017) Lithological influences on contemporary and long-term regolith weathering at the Luquillo Critical Zone Observatory. *Geochim. Cosmochim. Acta* 196, 224–251.
- Buss H. L., Mathur R., White A. F. and Brantley S. L. (2010) Phosphorus and iron cycling in deep saprolite, Luquillo Mountains, Puerto Rico. Chem. Geol. 269, 52–61.
- Chacon N., Silver W. L., Dubinsky E. A. and Cusack D. F. (2006) Iron reduction and soil phosphorus solubilization in humid tropical forests soils: the roles of labile carbon pools and an electron shuttle compound. *Biogeochemistry* **78**, 67–84.
- Chadwick O. A., Brimhall G. H. and Hendricks D. M. (1990) From a black to a gray box—a mass balance interpretation of pedogenesis. *Geomorphology* 3, 369–390.
- Chen C. R., Hou E. Q., Condron L. M., Bacon G., Esfandbod M., Olley J. and Turner B. L. (2015) Soil phosphorus fractionation and nutrient dynamics along the Cooloola coastal dune chronosequence, southern Queensland, Australia. *Geoderma* **257**, 4–13.
- Chen H.-Y., Fang T.-H., Preston M. R. and Lin S. (2006) Characterization of phosphorus in the aerosol of a coastal atmosphere: Using a sequential extraction method. *Atmos. Environ.* **40**, 279–289.
- Cotrufo M. F., Wallenstein M. D., Boot C. M., Denef K. and Paul E. (2013) The Microbial Efficiency-Matrix Stabilization (MEMS) framework integrates plant litter decomposition with soil organic matter stabilization: do labile plant inputs form stable soil organic matter? Glob. Chang. Biol. 19, 988–995.
- Crews T. E., Kitayama K., Fownes J. H., Riley R. H., Herbert D. A., Muellerdombois D. and Vitousek P. M. (1995) Changes in soil phosphorus fractions and ecosystem dynamics across a long chronosequence in Hawaii. *Ecology* 76, 1407–1424.
- Cross A. F. and Schlesinger W. H. (1995) A literature review and evaluation of the Hedley fractionation: applications to the biogeochemical cycle of soil phosphorus in natural ecosystems. *Geoderma* **64**, 197–214.

- Cross A. F. and Schlesinger W. H. (2001) Biological and geochemical controls on phosphorus fractions in semiarid soils. *Biogeochemistry* **52**, 155–172.
- Cui L. (2014) The Denudation Rates of Granite Region in Eastern China: Results of Cosmogenic Nuclides 10Be and 26Al. Institute of Geochemistry Chinese Academy of Sciences, Guiyang, Guizhou, pp. 1–96.
- Cui L., Liu C., Xu S., Zhao Z., Tu C., Liu T. and Ding H. (2014) The long-term denudation rate of granitic regolith in Qinhuangdao, North China determined from the in situ depth profile of the cosmogenic nuclides 26Al and 10Be. *Chin. Sci. Bull.* 59, 4823–4828.
- Deiss L., de Moraes A. and Maire V. (2018) Environmental drivers of soil phosphorus composition in natural ecosystems. *Biogeo-sciences* 15, 4575–4592.
- Dere A. L. (2014) Shale Weathering Across a Latitudinal Climose-quence. The Pennsylvania State University, pp. 1–302.
- Derry L. A. and Chadwick O. A. (2007) Contributions from Earth's atmosphere to soil. *Elements* 3, 333–338.
- Dixon J. L., Hartshorn A. S., Heimsath A. M., DiBiase R. A. and Whipple K. X. (2012) Chemical weathering response to tectonic forcing: A soils perspective from the San Gabriel Mountains, California. *Earth Planet. Sci. Lett.* 323–324, 40–49.
- Eger A., Almond P. C. and Condron L. M. (2011) Pedogenesis, soil mass balance, phosphorus dynamics and vegetation communities across a Holocene soil chronosequence in a super-humid climate, South Westland, New Zealand. *Geoderma* 163, 185– 196
- Eger A., Almond P. C. and Condron L. M. (2013) Phosphorus fertilization by active dust deposition in a super-humid, temperate environment—Soil phosphorus fractionation and accession processes. *Global Biogeochem. Cycl.* 27, 108–118.
- Elser J. J., Bracken M. E., Cleland E. E., Gruner D. S., Harpole W. S., Hillebrand H., Ngai J. T., Seabloom E. W., Shurin J. B. and Smith J. E. (2007) Global analysis of nitrogen and phosphorus limitation of primary producers in freshwater, marine and terrestrial ecosystems. *Ecol. Lett.* 10, 1135–1142.
- Emadi M., Baghernejad M., Bahmanyar M. A. and Morovvat A. (2012) Changes in soil inorganic phosphorous pools along a precipitation gradient in northern Iran. *Int. J. Forest. Soil Erosi.* 2, 143–147.
- Eriksson A. K., Hillier S., Hesterberg D., Klysubun W., Ulén B. and Gustafsson J. P. (2016) Evolution of phosphorus speciation with depth in an agricultural soil profile. *Geoderma* **280**, 29–37.
- FAO, 2015. Global forest resources assessment 2015, Available at: http://www.fao.org/resources/infographics/infographics-details/en/c/325836.
- Feng J., Turner B. L., Lü X., Chen Z., Wei K., Tian J., Wang C., Luo W. and Chen L. (2016) Phosphorus transformations along a large-scale climosequence in arid and semiarid grasslands of northern China. *Global Biogeochem. Cycl.* **30**, 1264–1275.
- Ferrier K. L., Kirchner J. W. and Finkel R. C. (2011) Estimating millennial-scale rates of dust incorporation into eroding hillslope regolith using cosmogenic nuclides and immobile weathering tracers. *J. Geophys. Res. Earth Surf.* 116.
- Filippelli G. M. (2008) The global phosphorus cycle: past, present, and future. *Elements* **4.** 89–95.
- Flaum J. A. (2008) Investigation of Phosphorus Cycle Dynamics Associated with Organic Carbon Burial in Modern (North Pacific) and Ancient (Devonian and Cretaceous) Marine Systems: Strengths and Limitations of Sequentially Extracted (SEDEX) Phosphorus Data. Northwestern University, Evanston, Illinois, pp. 1–196.
- Föllmi K. (1996) The phosphorus cycle, phosphogenesis and marine phosphate-rich deposits. *Earth Sci. Rev.* **40**, 55–124.

- Fox T. R. and Comerford N. B. (1990) Low-molecular-weight organic acids in selected forest soils of the southeastern USA. Soil Sci. Soc. Am. J. 54, 1139–1144.
- Gallardo A., Fernández-Palacios J. M., Bermúdez A., de Nascimento L., Durán J., García-Velázquez L., Méndez J. and Rodríguez A. (2020) The pedogenic Walker and Syers model under high atmospheric P deposition rates. *Biogeochemistry*, 1–17
- Glæsner N., van der Bom F., Bruun S., McLaren T., Larsen F. H. and Magid J. (2019) Phosphorus characterization and plant availability in soil profiles after long-term urban waste application. *Geoderma* 338, 136–144.
- Golchin A., Baldock J. and Oades J. (1997) A Model Linking Organic Matter Decomposition, Chemistry, and Aggregate Dynamics Soil Processes and the Carbon Cycle. CRC Press, Boca Raton, pp. 245–266.
- Goyne K. W., Brantley S. L. and Chorover J. (2006) Effects of organic acids and dissolved oxygen on apatite and chalcopyrite dissolution: Implications for using elements as organomarkers and oxymarkers. *Chem. Geol.* 234, 28–45.
- Gu C., Dam T., Hart S. C., Turner B. L., Chadwick O. A., Berhe A. A., Hu Y. and Zhu M. (2020) Quantifying uncertainties in sequential chemical extraction of soil phosphorus using XANES spectroscopy. *Environ. Sci. Technol.* 54, 2257–2267.
- Gu C., Hart S. C., Turner B. L., Hu Y., Meng Y. and Zhu M. (2019) Aeolian dust deposition and the perturbation of phosphorus transformations during long-term ecosystem development in a cool, semi-arid environment. *Geochim. Cosmochim. Acta* 246, 498–514.
- Hasenmueller E. A., Gu X., Weitzman J. N., Adams T. S.,
  Stinchcomb G. E., Eissenstat D. M., Drohan P. J., Brantley S.
  L. and Kaye J. P. (2017) Weathering of rock to regolith: The activity of deep roots in bedrock fractures. *Geoderma* 300, 11–31
- Hedley M. J., Stewart J. W. B. and Chauhan B. S. (1982) Changes in inorganic and organic soil phosphorus fractions induced by cultivation practices and by laboratory incubations. *Soil Sci. Soc. Am. J.* 46, 970–976.
- Heimsath A. M., DiBiase R. A. and Whipple K. X. (2012) Soil production limits and the transition to bedrock-dominated landscapes. *Nat. Geosci.* **5**, 210–214.
- Hesterberg D., Zhou W. Q., Hutchison K. J., Beauchemin S. and Sayers D. E. (1999) XAFS study of adsorbed and mineral forms of phosphate. J. Synchrotron Radiat. 6, 636–638.
- Holmgren G. G. S. (1967) A rapid citrate-dithionite extractable iron procedure. *Soil Sci. Soc. Am. J.* **31**, 210–211.
- Hooda P., Rendell A., Edwards A., Withers P., Aitken M. and Truesdale V. (2000) Relating soil phosphorus indices to potential phosphorus release to water. J. Environ. Qual. 29, 1166–1171.
- Hou E., Chen C., Luo Y., Zhou G., Kuang Y., Zhang Y., Heenan M., Lu X. and Wen D. (2018) Effects of climate on soil phosphorus cycle and availability in natural terrestrial ecosystems. *Glob. Chang. Biol.* 24, 3344–3356.
- Huang E., Chen Y., Schefuß E., Steinke S., Liu J., Tian J., Martínez-Méndez G. and Mohtadi M. (2018) Precession and glacial-cycle controls of monsoon precipitation isotope changes over East Asia during the Pleistocene. *Earth Planet. Sci. Lett.* 494, 1–11.
- Ingall E. D., Brandes J. A., Diaz J. M., de Jonge M. D., Paterson D., McNulty I., Elliott W. C. and Northrup P. (2011) Phosphorus K-edge XANES spectroscopy of mineral standards. J. Synchrotron Radiat. 18, 189–197.
- Ippolito J. A., Blecker S. W., Freeman C. L., McCulley R. L., Blair J. M. and Kelly E. F. (2010) Phosphorus biogeochemistry

- across a precipitation gradient in grasslands of central North America. J. Arid Environ. 74, 954-961.
- Izquierdo J. E., Houlton B. Z. and van Huysen T. L. (2013) Evidence for progressive phosphorus limitation over long-term ecosystem development: examination of a biogeochemical paradigm. *Plant. Soil.* 367, 135–147.
- Jenny H. (1941) Factors of Soil Formation: A System of Quantitative Pedology. McGraw-Hill Book Company Inc., New York.
- Jobbágy E. G. and Jackson R. B. (2001) The distribution of soil nutrients with depth: Global patterns and the imprint of plants. *Biogeochemistry* **53**, 51–77.
- Kar G., Hundal L. S., Schoenau J. J. and Peak D. (2011) Direct chemical speciation of P in sequential chemical extraction residues using P K-edge X-Ray absorption near-edge structure spectroscopy. Soil Sci. 176, 589–595.
- Koch M., Kruse J., Eichler-Löbermann B., Zimmer D., Willbold S., Leinweber P. and Siebers N. (2018) Phosphorus stocks and speciation in soil profiles of a long-term fertilizer experiment: Evidence from sequential fractionation, P K-edge XANES, and 31P NMR spectroscopy. *Geoderma* 316, 115–126.
- Kraal P., Bostick B. C., Behrends T., Reichart G.-J. and Slomp C. P. (2015) Characterization of phosphorus species in sediments from the Arabian Sea oxygen minimum zone: Combining sequential extractions and X-ray spectroscopy. *Mar. Chem.* 168, 1–8.
- Li J., Zhang G., Ruan L., Yang J. and Wang H. (2016) Sr-Nd elements and isotopes as tracers of dust input in a tropical soil chronosequence. *Geoderma* 262, 227–234.
- Li W., Liu X.-M. and Chadwick O. A. (2020) Lithium isotope behavior in Hawaiian regoliths: Soil-atmosphere-biosphere exchanges. *Geochim. Cosmochim. Acta* 285, 175–192.
- Liptzin D. and Silver W. L. (2009) Effects of carbon additions on iron reduction and phosphorus availability in a humid tropical forest soil. Soil Biol. Biochem. 41, 1696–1702.
- Mahowald N., Jickells T. D., Baker A. R., Artaxo P., Benitez-Nelson C. R., Bergametti G., Bond T. C., Chen Y., Cohen D. D., Herut B., Kubilay N., Losno R., Luo C., Maenhaut W., McGee K. A., Okin G. S., Siefert R. L. and Tsukuda S. (2008) Global distribution of atmospheric phosphorus sources, concentrations and deposition rates, and anthropogenic impacts. Global Biogeochem. Cycl. 22.
- Martens D. C., Lutz J. A. and Jones G. D. (1969) Form and availability of P in selected Virginia soils as related to available P tests. *Agron. J.* **61**, 616–621.
- Mattingly G. E. G. (1975) Labile phosphate in soils. *Soil Sci.* **119**, 369–375.
- McCulley R. L., Jobbagy E. G., Pockman W. T. and Jackson R. B. (2004) Nutrient uptake as a contributing explanation for deep rooting in arid and semi-arid ecosystems. *Oecologia* 141, 620–628
- McLennan S. M. (1993) Weathering and global denudation. *J. Geol.* **101**, 295–303.
- Miller A. J., Schuur E. A. G. and Chadwick O. A. (2001) Redox control of phosphorus pools in Hawaiian montane forest soils. *Geoderma* 102, 219–237.
- Mishra A., Tripathi J. K., Mehta P. and Rajamani V. (2013) Phosphorus distribution and fractionation during weathering of amphibolites and gneisses in different climatic setups of the Kaveri river catchment, India. Appl. Geochem. 33, 173–181.
- Murphy J. and Riley J. P. (1962) A modified single solution method for the determination of phosphate in natural waters. *Anal. Chim. Acta* 27, 31–36.
- Negassa W. and Leinweber P. (2009) How does the Hedley sequential phosphorus fractionation reflect impacts of land use and management on soil phosphorus: a review. *J. Plant Nutr. Soil Sci.* **172**, 305–325.

- Nesbitt H. W. and Young G. M. (1982) Early Proterozoic climates and plate motions inferred from major element chemistry of lutites. *Nature* 299, 715–717.
- Newman G. S., Coble A. A., Haskins K. E., Kowler A. L. and Hart S. C. (2020) The expanding role of deep roots during long-term terrestrial ecosystem development. *J. Ecol.* **108**, 2256–2269.
- Ni J., Lin P., Zhen Y., Yao X. and Guo L. (2015) Distribution, source and chemical speciation of phosphorus in surface sediments of the central Pacific Ocean. *Deep-Sea Res. Part I: Ocean. Res. Pap.* 105, 74–82.
- Parfitt R. L. (1989) Phosphate reactions with natural allophane, ferrihydrite and goethite. *J. Soil Sci.* **40**, 359–369.
- Pett-Ridge J. C. (2009) Contributions of dust to phosphorus cycling in tropical forests of the Luquillo Mountains, Puerto Rico. *Biogeochemistry* **94**, 63–80.
- Porder S. and Chadwick O. A. (2009) Climate and soil-age constraints on nutrient uplift and retention by plants. *Ecology* 90, 623–636.
- Prietzel J., Dümig A., Wu Y., Zhou J. and Klysubun W. (2013) Synchrotron-based P K-edge XANES spectroscopy reveals rapid changes of phosphorus speciation in the topsoil of two glacier foreland chronosequences. *Geochim. Cosmochim. Acta* 108, 154–171.
- Prietzel J. and Klysubun W. (2018) Phosphorus K-edge XANES spectroscopy has probably often underestimated iron oxyhydroxide-bound P in soils. J. Synchrotron Radiat. 25, 1736–1744.
- Prietzel J., Klysubun W. and Werner F. (2016) Speciation of phosphorus in temperate zone forest soils as assessed by combined wet-chemical fractionation and XANES spectroscopy. J. Plant Nutr. Soil Sci. 179, 168–185.
- Ravel B. and Newville M. (2005) ATHENA, ARTEMIS, HEPHAESTUS: data analysis for X-ray absorption spectroscopy using IFEFFIT. J. Synchrotron Radiat. 12, 537–541.
- Rea P., Ma L., Gill T. E., Gardea-Torresdey J., Tamez C. and Jin L. (2020) Tracing gypsiferous White Sands aerosols in the shallow critical zone in the northern Sacramento Mountains, New Mexico using Sr/Ca and 87Sr/86Sr ratios. *Geoderma* 372 114387.
- Riebe C. S., Hahm W. J. and Brantley S. L. (2017) Controls on deep critical zone architecture: a historical review and four testable hypotheses. *Earth Surf. Processes Landforms* 42, 128– 156.
- Riebe C. S., Kirchner J. W. and Finkel R. C. (2003) Long-term rates of chemical weathering and physical erosion from cosmogenic nuclides and geochemical mass balance. *Geochim. Cosmochim. Acta* 67, 4411–4427.
- Riebe C. S., Kirchner J. W., Granger D. E. and Finkel R. C. (2001) Strong tectonic and weak climatic control of long-term chemical weathering rates. *Geology* 29, 511–514.
- Robertson G. P., Coleman D. C., Bledsoe C. S. and Sollins P. (1999) Standard Soil Methods for Long-term Ecological Research. Oxford University Press, New York.
- Rowarth J. S. and Tillman R. W. (1992) A glasshouse evaluation of plant availability of soil phosphate fractions. N.Z. J. Agric. Res. 35, 329–336.
- Sardans J. and Peñuelas J. (2014) Hydraulic redistribution by plants and nutrient stoichiometry: shifts under global change. *Ecohydrology* 7, 1–20.
- Sato S., Solomon D., Hyland C., Ketterings Q. M. and Lehmann J. (2005) Phosphorus speciation in manure and manure-amended soils using XANES spectroscopy. *Environ. Sci. Technol.* 39, 7485–7491.
- Scholes R. J. and Archer S. R. (1997) Tree-grass interactions in savannas. *Annu. Rev. Ecol. Syst.* 28, 517-544.

- Schwertmann U. (1964) Differentiation of soil iron oxides by extraction with ammonium oxalate-solution. Z. Pflanzenernähr. Düng. Bodenkd. 105, 194–202.
- Shen Z. X., Cao J. J., Arimoto R., Zhang R. J., Jie D. M., Liu S. X. and Zhu C. S. (2007) Chemical composition and source characterization of spring aerosol over Horqin sand land in northeastern China. J. Geophys. Res. 112, D14315.
- Soil Survey Staff (2014) Keys to Soil Taxonomy, 12th ed. United States Department of Agriculture, Natural Resources Conservation Service, Washington, DC.
- Spohn M. (2020) Increasing the organic carbon stocks in mineral soils sequesters large amounts of phosphorus. *Glob. Chang. Biol.* **00**, 1–9.
- St. Arnaud R. J., Stewart J. W. B. and Frossard E. (1988) Application of the 'Pedogenic Index' to soil fertility studies, Saskatchewan. *Geoderma* 43, 21–32.
- Tiessen H. and Moir J. O. (1993) Characterization of available phosphorus by sequential extraction. In *Soil Sampling and Methods of Analysis* (ed. M. R. Carter). Lewis, Chelsea, MI, pp. 75–86.
- Tipping E., Somerville C. J. and Luster J. (2016) The C:N:P: S stoichiometry of soil organic matter. *Biogeochemistry* **130**, 117–131
- Turner B. L. and Laliberté E. (2015) Soil development and nutrient availability along a 2 million-year coastal dune chronosequence under species-rich Mediterranean shrubland in southwestern Australia. *Ecosystems* 18, 287–309.
- Tyrrell T. (1999) The relative influences of nitrogen and phosphorus on oceanic primary production. *Nature* **400**, 525–531.
- Vitousek P. M., Porder S., Houlton B. Z. and Chadwick O. A. (2010) Terrestrial phosphorus limitation: mechanisms, implications, and nitrogen-phosphorus interactions. *Ecol. Appl.* 20, 5– 15
- Vitousek P. M. and Sanford R. L. (1986) Nutrient cycling in moist tropical forest. Annu. Rev. Ecol. Syst. 17, 137–167.
- Walker T. W. and Syers J. K. (1976) The fate of phosphorus during pedogenesis. *Geoderma* 15, 1–19.
- Wang X., Hu Y., Tang Y., Yang P., Feng X., Xu W. and Zhu M. (2017) Phosphate and phytate adsorption and precipitation on ferrihydrite surfaces. *Environ. Sci. Nano* 4, 2193–2204.
- Welch S. A., Taunton A. E. and Banfield J. F. (2002) Effect of microorganisms and microbial metabolites on apatite dissolution. *Geomicrobiol. J.* 19, 343–367.
- Weng L., Vega F. A. and Van Riemsdijk W. H. (2011) Competitive and synergistic effects in pH dependent phosphate adsorption in soils: LCD modeling. *Environ. Sci. Technol.* 45, 8420–8428.
- Werner F., de la Haye T. R., Spielvogel S. and Prietzel J. (2017) Small-scale spatial distribution of phosphorus fractions in soils from silicate parent material with different degree of podzolization. *Geoderma* 302, 52–65.
- Xie Y. and Chi Y. (2016) Geochemical investigation of dry- and wet-deposited dust during the same dust-storm event in Harbin, China: Constraint on provenance and implications for formation of aeolian loess. J. Asian Earth Sci. 120, 43–61.
- Zhang Z., Goldstein H. L., Reynolds R. L., Hu Y., Wang X. and Zhu M. (2018) Phosphorus speciation and solubility in aeolian dust deposited in the interior American West. *Environ. Sci. Technol.* 52, 2658–2667.
- Zhou Y., Boutton T. W. and Wu X. B. (2018) Woody plant encroachment amplifies spatial heterogeneity of soil phosphorus to considerable depth. *Ecology* 99, 136–147.